Journal of Visualized Experiments

Stress distribution during cold compression of rocks and mineral aggregates using synchrotron based X-ray diffraction
--Manuscript Draft--

Article Type:	Invited Methods Article - JoVE Produced Video
Manuscript Number:	JoVE57555R2
Full Title:	Stress distribution during cold compression of rocks and mineral aggregates using synchrotron based X-ray diffraction
Keywords:	rock mechanics; compaction; stress; strain; High Pressure; X-ray Diffraction; synchrotron radiation; multi-anvil cell; crystallography; mineralogy; geophysics; Mineral Physics
Corresponding Author:	Cecilia S. N. Cheung University of Wisconsin Madison College of Engineering Stony Brook, NY UNITED STATES
Corresponding Author's Institution:	University of Wisconsin Madison College of Engineering
Corresponding Author E-Mail:	scheung9@wisc.edu
First Author:	Cecilia S. N. Cheung
Other Authors:	Donald J. Weidner
	Li Li
	Philip G. Meredith
	Haiyan Chen
	Matthew Whitaker
	Xianyin Chen
Author Comments:	
Additional Information:	
Question	Response
If this article needs to be "in-press" by a certain date, please indicate the date below and explain in your cover letter.	

TITLE:

Stress Distribution During Cold Compression of Rocks and Mineral Aggregates Using Synchrotron-Based X-Ray Diffraction

AUTHORS & AFFILIATIONS:

Cecilia S N Cheung[1,2], Donald J Weidner[1], Li Li[1], Philip G Meredith[3], Haiyan Chen[1], Matthew L Whitaker[1], Xianyin Chen[4]

[1]Mineral Physics Institute, Department of Geoscience, Stony Brook University, Stony Brook, NY, USA 11794-2100

[2]Geological Engineering, Department of Civil and Environmental Engineering, University of Wisconsin-Madison, Madison, USA 53706-1691

[3]Rock and Ice Physics Laboratory, Department of Earth Sciences, University College London, London, UK

[4]Department of Chemistry, Stony Brook University, Stony Brook, NY, USA 11794-2100

Corresponding Author:

Cecilia S N Cheung

Email Address: scheung9@wisc.edu

Tel: (631)-413-4842

Email Addresses of Co-authors**:**

Donald J Weidner (donald.weidner@stonybrook.edu)

Li Li (li.li.2@stonybrook.edu)

Philip G Meredith (p.meredith@ucl.ac.uk)

Haiyan Chen (haiyan@bnl.gov)

Matthew L Whitaker (matthew.whitaker@stonybrook.edu)

Xianyin Chen (xianyin.chen@stonybrook.edu)

KEYWORDS:

Rock mechanics, compaction, stress, strain, high pressure, X-ray diffraction, synchrotron radiation, multi-anvil cell, crystallography, mineralogy, geophysics, mineral physics

SHORT ABSTRACT:

We report detailed procedures for compression experiments on rocks and mineral aggregates within a multi-anvil deformation apparatus coupled with synchrotron X-radiation. Such experiments allow quantification of the stress distribution within samples, that ultimately sheds light on compaction processes in geomaterials.

LONG ABSTRACT:

We report detailed procedures for performing compression experiments on rocks and mineral aggregates within a multi-anvil deformation apparatus (D-DIA) coupled with synchrotron X-radiation. A cube-shaped sample assembly is prepared and compressed, at room temperature, by a set of four X-ray transparent sintered diamond anvils and two tungsten carbide anvils, in the lateral and the vertical planes, respectively. All six anvils are housed within a 250-ton hydraulic

press and driven inward simultaneously by two wedged guide blocks. A horizontal energy dispersive X-ray beam is projected through and diffracted by the sample assembly. The beam is commonly in the mode of either white or monochromatic X-ray. In the case of white X-ray, the diffracted X-rays are detected by a solid-state detector array that collects the resulting energy dispersive diffraction pattern. In the case of monochromatic X-ray, the diffracted pattern is recorded using a two-dimensional (2-D) detector, such as an imaging plate or a charge-coupled device (CCD) detector. The 2-D diffraction patterns are analyzed to derive lattice spacings. The elastic strains of the sample are derived from the atomic lattice spacing within grains. The stress is then calculated using the predetermined elastic modulus and the elastic strain. Furthermore, the stress distribution in two-dimensions allow for understanding how stress is distributed in different orientations. In addition, a scintillator in the X-ray path yields a visible light image of the sample environment, which allows for the precise measurement of sample length changes during the experiment, yielding a direct measurement of volume strain on the sample. This type of experiment can quantify the stress distribution within geomaterials, which can ultimately shed light on the mechanism responsible for compaction. Such knowledge has the potential to significantly improve our understanding of key processes in rock mechanics, geotechnical engineering, mineral physics, and material science applications where compactive processes are important.

INTRODUCTION:
The rationale behind the method presented in this article is to quantify the stress distribution within rock and mineral aggregate samples during compression and subsequent compaction. Understanding the compaction in rocks and mineral aggregates is of great importance to reservoir and geotechnical engineering[8,17-20,28,33]. Compaction acts to reduce porosity, and therefore, leads to an increase in pore pressure. Any such increase in pore pressure leads to a decrease in effective pressure[35]. The consequence is that it will significantly weaken the reservoir rock, and can therefore be subjected to premature failure at lower stress. Some examples of the resulting consequences of inelastic deformation in the subsurface include: failure in sustaining long term production in oil and gas reservoirs[28,33], surface subsidence[8,18-20], and alteration of fluid flow patterns[17]. Therefore, a comprehensive knowledge of compaction processes in rocks and mineral aggregates could aid in reducing the possibility of such potentially negative consequences.

The great advantage of using the method highlighted here is that it provides a means to quantify stress distribution internally within a geomaterial[5-6] with respect to the globally-averaged externally applied pressure[12,22]. Moreover, as an *in situ* experiment, the evolution of the stress distribution is time-resolved. The externally applied pressures considered range from relatively low values (tens of megapascals) to high values (several gigapascals). The stress within the sample is measured indirectly by using the atomic lattice spacing within individual mineral grains as a measure of the local elastic strain[5-6]. The atomic lattice spacing is determined with the aid of X-radiation, commonly in either the mode of white or monochromatic X-ray. For the white X-ray mode (*e.g.,* DDIA at 6BM-B beamline of the Advanced Photon Source (APS), Argonne National Laboratory), the intensity of the diffracted beam X-ray beam is determined by not just one, but by an array of 10-element Ge detectors (**Figure 1**) distributed along a fixed circle at azimuthal

89 angles of 0°, 22.5°, 45°, 67.5°, 90°, 112.5°, 135°, 157.5°, 180°, 270°. For the monochromatic X-ray
90 mode, the diffracted pattern is recorded using a CCD detector (*e.g.,* DDIA-30 at 13-ID-D beamline
91 of the GSECARS, APS, Argonne National Laboratory)[18,23]. Both X-ray modes allow quantification
92 on how the stress varies in different orientations. This approach is fundamentally different from
93 all previous studies of compaction in geomaterials.
94
95 In typical compaction studies, a cylindrical sample is compressed by an axial force that is applied
96 across the cross-sectional area by the actuator[25]. Under such conditions, the magnitude of the
97 applied stress magnitude is generally calculated by simply dividing the axial force (measured by
98 a load cell) by the initial cross-sectional area of the sample. It should be noted that this applied
99 stress magnitude is merely an average, bulk value and, as such, does not realistically represent
100 how the local stress state varies, or is distributed, within a complex, heterogeneous, granular
101 material. Detrital sedimentary rocks, which are examples of complex granular materials, are
102 formed by aggregation of mineral grains that are subsequently compacted and cemented
103 through depositional and diagenetic processes[1,7,21,30-31]. These aggregates naturally inherit pores
104 that comprise the void spaces between grains, which are intrinsic from the geometry of grain
105 packing modified by secondary dissolution. Hence, any applied stress is expected to be supported
106 by and concentrated at grain-to-grain contacts, and to vanish at grain-pore interfaces.
107
108 In addition to the complexity of stress variation within a granular material, other factors further
109 complicate studying compaction in these scenarios. First, the local stress field is vulnerable to
110 any changes due to microstructural artifacts (*e.g.,* grain shape, preexisting fractures) that are
111 inevitably present within any detrital sedimentary rock. Second, although the magnitude of the
112 applied stress acting upon the sample surfaces can be fully quantified, the distribution of stresses
113 within the sample body remained poorly constrained. An end effect[32] — a boundary effect
114 whereby the average stress is concentrated near the contact between the loading rams and the
115 samples due to interface friction — is well known to be exhibited in cylindrical samples loaded in
116 compression. As an example, Peng[26] demonstrated strain heterogeneity within uniaxially
117 compressed granite samples subjected to a variety of end conditions. Hence, to accurately
118 compute the local stress distribution in granular material, we present the following detailed
119 protocol for performing X-ray diffraction (XRD) experiments on rocks and mineral aggregates,
120 using a multi-anvil deformation apparatus at beamline 6-BM-B of the APS at Argonne National
121 Laboratory.
122
123 **PROTOCOL:**
124
125 **1. Sample Preparation**
126
127 1.1. Choose the test and/or reference sample; this can be either a rock core (step 1.2) or a mineral
128 aggregate (step 1.3), depending the focus of the experimental study.
129
130 Note: The following method is certainly not the only way to prepare good quality samples (*e.g.,*
131 other machines can be used). However, the sample preparation adopted in the present study is
132 fully illustrated to achieve the goal of accurate replication.

1.2. Rock core samples

1.2.1. Saw a small rectangular slab from a larger sample rock block. Then surface grind the sample slab such that all six surfaces of the slab are flat and perpendicular to their adjacent surfaces.

1.2.2. To minimize any movement of the sample slab during core drilling, start by placing a machine vice (**Figure 2a**) on a working surface that is highly stable. Ensure that all contact surfaces are clean so that non-perpendicularity is not introduced to the setup. Place the sample slab between the vice jaws (**Figure 2a**) and screw the jaws together ensuring that they are just tight enough to secure the sample without damaging it.

1.2.3. Setup a rotatory tool with a rotatory workstation package as a coring drill press (**Figure 2a**). Insert a 2 mm (inner diameter) coring diamond drill bit into an adjustable chuck of the drill press. Screw and lock the core drill bit to ensure the assembly is stable during drilling.

1.2.4. Turn on the rotatory tool and start lowering the drill assembly towards the sample slab.

Note: Heat is produced at the drill bit tip as the drilling progresses. Excess heat could cause the diamonds at the drill bit tip to wear at an accelerated rate. Since the rotatory drill press is not equipped with a water cooling system, and since our sample size is in the millimeter range, the drill bit can be cooled by injecting coolant manually onto the contact between the rotating drill bit and the slab.

1.2.5. Drill to the depth of at least 3.25 mm (double of the ideal final height of the sample) so that substantial height is left for end surface preparation afterwards.

1.2.5.1. If after retracting the drill bit, the drilled core is still attached to the sample slab, then insert the drill bit around the core and wiggle it slowly until the core is detached from the slab.

1.2.5.2. If the drilled core is already detached and stuck in the interior of the core drill bit, then insert a pin of diameter 1.85 mm from the opposite end to push the core towards the outside for retrieval.

1.2.6. Use wipes to dry the cooling water, and then air dry the retrieved samples for at least 2 h or, if possible, overnight. Clean the ground dust around the core by rolling it on a piece of low adhesive tape. Measure the diameter of the core and prioritize the samples by a diameter closest to 1.9+ mm.

1.2.7. Next prepare for surface grinding of the end surfaces**.**

Note: It is **extremely important** to have the end surface contacts flat so that the applied load can be evenly distributed across the entire surface area.

177 1.2.7.1. Place sand paper under the grinding jig (**Figure 2b**). Start grinding with coarse grit (*e.g.,*
178 600 grit), progress towards a finer grit, and finish with at least a 1,500 grit. Insert the core into
179 one end of the hole of the grinding jig. Place tape around the core if it does not fit tightly into the
180 hole of the jig.

181

182 Note: Ensure the work surface remains clean to ensure perpendicularity.

183

184 1.2.7.2. Insert a pin (diameter of 1.4 mm) into the other end of the hole. Keep holding the pin
185 gently downwards to keep the sand paper and core in contact (**Figure 2b**). Maintain this position
186 and start slowly grinding the core against the sand paper. Take the core out of the jig and check
187 often to see if the final height (1.67 mm) is reached and if the surface is even.

188

189 1.2.7.3. For parallelism, insert the sample back to the jig for further grinding, until it reaches a
190 precision within 0.5°.

191

192 1.2.8. To assist in deciding on which sample is the best to use, check the overall shape of the
193 samples using a low magnification (2X–8X) microscope. If possible, obtain some microscopic
194 photographs of the samples for documentation as well.

195

196 **1.3. Mineral aggregate samples**

197

198 **1.3.1. Prepare mineral grains by first grinding a suitably sized sample of rock or pre-existing**
199 **powder in a pestle and mortar.**

200

201 Note: This process can be sped up by using a rotatory tool with a grinding head, instead of the
202 pestle.

203

204 1.3.2. Use a low magnification microscope to measure the grain size. Continue grinding until the
205 average diameter of the grains is 4 μm.

206

207 **1.3.2.1. Suspend the grains in ethanol. Then separate the grains from the ethanol suspension by**
208 **using a tall decantation column (~20 cm in height) and settling by gravity.**

209

210 Note: The removal of grains that are smaller and larger than 4 μm (± 0.5 μm), is based on their
211 mass. The gravitational force acting on the grain is given by:

212

213 $$F_{gravity} = mg$$

214

215 where m is the mass, and g is the acceleration due to gravity. The forces opposing the motion are
216 buoyancy and drag force. The buoyancy force is given by Archimedes' principal:

217

218 $$F_{buoyancy} = \rho g V$$

219

220 where ρ is the density, and V is the volume of the displaced fluid. The drag force is given by:

$$F_{drag} = C_D[\frac{u^2}{2}]\rho A_p$$

where u is the particle-fluid relative velocity, A_p is the area of the particle projected in direction of the motion, and C_D is the drag coefficient. By balancing the forces, set the boundary condition at which the grains reach the terminal velocity. Assuming laminar flow conditions, the velocity of the grain v_{grain} is given in the resulting equation known as Stokes' Law:

$$v_{grain} = \sqrt{\frac{\rho - \rho_{ethanol}}{\rho_{ethanol}}} \times gd$$

where d is the diameter of the grain.

1.3.3. Extract the ethanol/grain mix at different heights in the column into separate glass beakers, to obtain grains sorted by their grain diameter.

Note: The rate of grain settling depends on its diameter and density.

1.3.4. Leave the content in the beakers overnight to air dry. Measure the final average diameter of the grains using a low magnification microscope and select the batch of grains with a diameter closest to 4 μm (for optimal X-ray signals).

2. Cell Assembly Preparation

2.1. Load the prepared samples into a standard D-DIA cell assembly (**Figure 3a**).

Note: The D-DIA cell assembly was developed under the Consortium for Materials Properties Research in Earth Sciences (COMPRES) multi-anvil cell assembly development project[14]. The following description of the standard D-DIA cell design (under the COMPRES project) can be used for an addition of increased temperature if desired.

2.1.1. Start with a cell assembly cube (6.18 mm edge length; **Figure 3**) on a clean working surface.

2.1.2. Clean an alumina rod (diameter of 1.5 mm, height of 1.46 mm; **Figure 3a**), an alumina ring (**Figure 3a**), and a graphite ring (**Figure 3a**) in an ultrasonic bath. Prepare the end surfaces of the alumina rod flat and parallel to a precision within 0.5° (refer to Section 1.2.7).

2.1.3. Put a piece of tape at one end of the hole of the cube. Use a pair of tweezers to put the two rings around the alumina rod, and insert them all the way down into the hole of the cube, and such that the graphite ring is in contact with the tape.

Note: The alumina ring is used as a separator; the graphite ring is used for electrical conductivity

262 upon higher temperature application (not applied for the cold compression presented in this
263 study).

264

265 2.1.4. Mark the corner of the cube to be aligned with the incoming X-ray beam direction (**Figure
266 4b**).

267

268 Note: The tantalum foil is used to obtain better contrast for quantifying the sample volume using
269 radiography during the experiment (Section 3).

270

271 2.1.4.1. Cut a rectangular piece of tantalum foil (1.5 mm x 17 mm). Fold the foil into a U-shape
272 piece (see **Figure 3b** for more details) and place inside the cylindrical space of the cell assembly.
273 To ensure a tight fit between the foil and the edges of the cylindrical space, use a pin (diameter
274 of 1.83 mm) to push onto the foil against the edges to remove any excess space between the
275 two.

276

277 2.1.4.2. Align this U-shaped foil with respect to the X-ray beam direction (**Figure 4a**), and aim to
278 minimize and maximize the 2-D projection of the foil and the samples, respectively.

279

280 2.1.5. Lay a piece of rectangular tantalum foil (1.7 mm x 1 mm) on top of the rock core (**Figure
281 3b**). Make sure the foil is flat, and align the foil such that the length (1.7 mm) of the foil is
282 perpendicular to the X-ray beam direction (**Figure 4a**).

283

284 Note: Either a rock core or mineral aggregate can be a "reference sample", depending on the
285 goal of the experimental study. In this particular example, insert the rock core prepared in Section
286 1.2. as the "reference sample" portion in **Figure 3b**. The purpose of this piece of foil is to provide
287 better contrast of the boundary between adjacent samples.

288

289 2.1.6. Carefully pack the mineral aggregate (prepared in Section 1.3) into the cylindrical space
290 with a spatula (the "sample" portion in **Figure 3b**).

291

292 Note: Again, either a rock core or mineral aggregate can be a "sample", depending on the goal of
293 the experimental study.

294

295 2.1.7. Remove the excess grains adhered to the lateral side of the cylindrical space gently with
296 air if necessary. Use a pin (diameter of 1.83 mm) and a caliper to check if the final height has
297 been reached; leave 1.4 mm in the height for inserting the top alumina rod.

298

299 2.1.8. Insert another rectangular piece of tantalum foil (1.7 mm x 1 mm). Clean a new set of an
300 alumina rod (diameter of 1.5 mm, height of 1.46 mm), an alumina ring, and a graphite ring (**Figure
301 3a**) in the ultrasonic bath. Use a pair of tweezers to put the two rings around the alumina rod,
302 and insert them such that remaining space of the cylindrical volume is fully filled with the graphite
303 ring on top.

304

305 2.1.9. Use a minimal amount of cement (zirconium powder mixed with activator) to seal the

alumina rod exposed on both ends of the cube. After the cement is dried, trim the excess tantalum foil that is still exposed outside of the cube for tidiness.

3. Experimental Procedure

Note: The following experiment is performed at beamline 6-BM-B (**Figure 4a**) of the APS at Argonne National Laboratory. The experiment performed at 6-BM-B is under white X-ray mode. This beamline is an open beamline and welcomes proposals from scientists, researchers, and students worldwide to perform experiments under its general user program.

3.1. Perform the energy calibration of the system by collecting a diffraction pattern for an alumina standard.

3.1.1. Collect a diffraction pattern by clicking the **start** button on the **12 Element Detector Control Pump** panel.

3.1.2. Analyze the alumina XRD pattern, which contains built-in Cobalt-57 (Co-57) fluorescence peaks, by calculating the average peak position (Horiz X, Vert Y, and Beam Z dimensions) over the different detectors.

3.1.3. Enter the average values as new pedestal positions in the **6motors.adl** panel. Recollect a diffraction pattern and save as an energy dispersive diffraction file (EDF), which constrains the 2-theta angle and the correlation function between the detector channel and X-ray energy for each of the 10 detectors.

3.2. Remove the alumina standard and collect an open press X-ray spectrum by clicking the **start** button on the **12 Element Detector Control Pump** panel (with an exposure time of 500 s, to optimize signal-to-noise ratio) to measure the diffraction of the background without any sample assembly.

3.3. Clean the anvils (truncation edge length of 4 mm) with acetone and use a portable vacuum cleaner to remove all debris from previous experiments. Insert the sample assembly prepared in Section 2 into the center of the experiment setup that consists of four, X-ray transparent, sintered diamond and two tungsten carbide (top/bottom) anvils (**Figure 4b**).

3.4. Slowly lower the opposing pairs of lateral anvils simultaneously. Use a level to check if the anvils are leveled. Gently push the anvil to adjust the alignment until it is all leveled. The bottom and four lateral anvils should now all be in contact with the sample assembly. Release the safety latch and insert the spacer (**Figure 4a**).

3.5. Close the hutch and enable the shutter to allow the X-ray beam to enter the hutch.

3.6. In the **low-pressure pump panel** (labeled as the pump motor controller module in **Figure 5**), turn the **low-pressure pump** button ON and push the **up** button next to the **top ram** label to

move the top ram to the top, against the spacer (**Figure 4a**). With the aid of real-time X-radiographic imaging (**Figure 5**), start moving the bottom ram up slowly and carefully until the anvils start to appear in the radiograph. **Leave a very fine gap** such that the sample is not overloaded initially before the experiment.

3.7. Turn off all the controls on the low-pressure pump controller module (**Figure 5**) and close the "pressurize" valve before starting to compress with the high-pressure hydraulic pump.

Note: The high-pressure pump is controlled using EPICS-based software (**Figure 5**). EPICS is a non-commercial set of open source software tools, libraries, and applications developed by Argonne National Laboratory.

3.7.1. Move the sample position in the Z direction (parallel to the beam) using the **jog** button in the **6motors.adl** panel such that the center of the sample in the ImageJ EPICS area detector plugin software panel aligns with the diffraction focus mark on the screen. This minimizes parasitic diffraction and optimizes the signal-to-noise ratio.

3.8. Collect diffraction spectra by clicking the **start** button on the **12 Element Detector Control Pump** panel for the core and the aggregate (**jog** button along pedestal Z to move between samples) separately, each with an exposure time of 500 s, at ambient conditions. On the **NDFileTIFF.adl** panel, click the **capture-start** button to capture a radiograph (**Figure 5**) of these samples with an exposure time of ~6 ms.

3.9. Drive the anvils inwards by wedged guide blocks running on the hydraulics pump by starting the motor. In the **SAM-85 Press Load Control** window (**Figure 6**), set the target load to 50 tons. Turn the feedback on, with the upper limit of the speed control set to 7 (the slowest compression possible).

Note: The press load and speed can be changed depending on the target pressure and the speed of the compression. The maximum press load to avoid the breakage of anvils is 100 tons.

3.10. Use the **Diffraction-Imaging-Scan-Prosilica** panel (**Figure 7**) to set up an automatic data collection by defining the desired locations of the core (*e.g.,* Press X = 20.738 mm, Press Y = 4.3 mm) and the aggregate (*e.g.,* Press X = 20.738 mm, Press Y = 4.8 mm) for diffraction (with preset exposure times of 500 s) and X-radiographic imaging. Set the cycles required to 0 such that this data collection will repeat continuously. Click **start** to start the data collection.

Note: As the compression progresses, the sample will move upwards, so new desired locations should be updated accordingly.

3.11. After reaching the target load of 50 ton, click the **stop** button to stop the automatic data collection in the **Diffraction-Imaging-Scan-Prosilica** panel (**Figure 7**). In the **SAM-85 Press Load Control** window, decompress the sample by setting the lower limit of the speed control to -10 and change the target load to 0 ton.

394

395 **3.12.** After unloading, collect the diffraction spectra for the core and the aggregate separately,
396 by clicking the **start** button on the **12 Element Detector Control Pump** panel; use an exposure
397 time of 500 s for both the core and the aggregate. On the **NDFileTIFF.adl** panel, click the **capture-**
398 **start** button to capture a radiograph (**Figure 5**) of these samples with an exposure time of ~6 ms.

399

400 **3.13.** In the low-pressure pump panel (labeled as the pump motor controller module in **Figure 5**),
401 open the **pressurize valve**. Push the **low-pressure pump – on** button. Press the **down** buttons
402 both next to the **top ram** and **bottom ram** labels to move both the top and the bottom ram
403 downwards until the green **Down** light becomes illuminated, then stop driving both rams.

404

405 **3.14.** In the **low-pressure pump** panel, press the **out** button near the **spacer block** label to move
406 the spacer arm to the **out** position, and then press the **up** button near the **top ram** label to drive
407 the top ram up until the safety lock engages. Turn all the controls off in the pump motor
408 controller unit (**Figure 5**) afterwards. Slowly and manually move the lateral anvils outwards and
409 remove the sample assembly.

410

411 **REPRESENTATIVE RESULTS:**
412 We show one representative result example from an XRD experiment (experiment SIO2_55) run
413 in the multi-anvil press at 6BM-B on a compound quartz aggregate[5,6] and novaculite core
414 sample[6]. The grain sizes of the quartz aggregate and novaculite are ~4 μm and ~6–9 μm,
415 respectively[5-6]. Selected diffraction spectra collected during this experiment are illustrated in
416 **Figure 8**. At ambient pressure, the diffraction spectra from the quartz aggregate and the
417 novaculite are essentially indistinguishable (experiment SIO2_55peak2-Set1 **Figure 8**).
418 Specifically, the relative intensities as well as the widths and positions of all the diffraction peaks
419 are indistinguishable between the two geo-materials. During subsequent compression, the peak
420 width remains unchanged for the novaculite with increasing pressure. In contrast, however, the
421 peak width broadens substantially for the quartz aggregate. **Figure 8** highlights the evolution of
422 the quartz aggregate peaks with increasing pressure; both axial and transverse peaks broaden
423 substantially with increasing pressure. The novaculite peak at zero pressure is also plotted in
424 **Figure 8** for comparison. As the pressure is increased, the peak position (*i.e.,* the centroid of the
425 peak) shifts to higher energy for the quartz aggregate (simultaneously, the novaculite peak shifts
426 to high energy, however, for simplicity, it is not shown in this figure). Higher energy is equivalent
427 to lower d-spacing but, for consistency, the low d-spacing edge of the peak is referred as the
428 high-energy or high-pressure side in this article. At pressures higher than P = ~0.9 gigapascals
429 (GPa) (experiment SIO2_55peak2-Set9 in **Figure 8**), the peak broadens remarkably with
430 increasing pressure for quartz aggregate on the high-energy side, while essentially not changing
431 on the low-energy side; this results in an asymmetric peak evolution. The quartz aggregate peak
432 appears to continue broadening, in both the axial and transverse directions, even at the highest
433 pressures achieved in this experiment of P = ~5.6 GPa (experiment SIO2_55peak2-Set15 in **Figure**
434 **8**). In contrast, the novaculite peak remains essentially the same shape as that at zero pressure
435 throughout (note that the novaculite peak at zero pressure is shown throughout **Figure 8** for
436 simplicity).

437

438 Since the peak position is an indicator of how close the lattice planes are to each other, a material
439 that contains grains with widely distributed lattice spacings will produce a broadened diffraction
440 peak, and vice versa. In essence, a broadened peak is a convoluted signal of the distribution of
441 lattice spacings in the sample and the instrument response[13]. After deconvolution, a wide
442 distribution of lattice spacings essentially implies a larger strain variance deviated from the mean
443 strain within the sample. This strain heterogeneity within the sample is a result of a stress
444 heterogeneity; hence, the broadening of the diffraction peaks can be used to reveal the
445 microstress distribution (differential stress) in the sample[41]. The micro-stress is estimated by
446 quantifying the width of the peak measured at half of the maximum peak height, commonly
447 referred as "full width half maximum" (FWHM) of the diffraction peak. As an illustration, FWHM
448 is marked as a green horizontal line between two vertical lines constraining the upper and lower
449 energy bounds for experiment SIO2_55peak2-Set1 in **Figure 8**. The FWHM is quantified by the
450 difference between the two energy bounds (*i.e.,* ~0.4 kiloelectron volt (keV) in this particular
451 example). If there is no detectable peak broadening due to change in the grain size ($W_d^2 = 0$; see
452 the **Discussion** for more details), the peak broadening due to strain (W_s^2) is the subtraction of the
453 total observed FWHM (W_o^2) and the response due to the instrumentation (W_i^2). The response
454 due to the instrumentation can be calculated from the open press spectra (Section 3.1.1). The
455 broadening due to strain (W_2) can be measured in unit of length of lattice spacing,

456

457
$$Strain = \frac{W_s}{d}$$

458

459 where *d* is the hydrostatic lattice spacing. Differential stress is given by,

460

462
$$Differential\ stress = E \times \frac{W_s}{d}$$

461

463 where *E* is the Young's modulus (the Voight-Reuss-Hill Average of Young's modulus for quartz is
464 adopted in this calculation[34]). For special case, if the stress in the grains of the sample can be
465 represented by a Gaussian distribution, then half of the grains within the sample will be at a
466 differential stress exceeding this mean value[41-42]. The remaining half of the grains will be at a
467 differential stress below this mean value.

468

469 The differential stress, as illustrated in **Figure 9**, is determined by using the peak broadening
470 method ($E \times W_s/d$)[41], for both the quartz aggregate and the novaculite as a function of pressure.
471 Although the plotted values are calculated from only the [101] peak (which is the diffraction peak
472 corresponding to the reflection of the [101] crystallographic planes), it should be noted that the
473 other peaks yield similar results. The novaculite peaks show virtually no broadening and hence
474 reflects that novaculite has accumulated only a modest amount of differential stress. On the
475 other hand, the quartz aggregate shows extremely large differential stresses in both the axial and
476 transverse directions. Moreover, there is twice the amount of the differential stress in the
477 transverse direction than that in the axial direction. In other words, the transverse direction is
478 supporting a significantly higher load as compared to the axial direction, since the load is the
479 driving force for the differential stress. It should be noted that the differential stress

480 ('microstress'), calculated using the above peak broadening method[41], reflects the local grain-to-
481 grain interactions and is not influenced by sample geometry. Such advantages are beneficial over
482 stress ('macrostress') calculated using lattice spacings[35].
483

484 As noted earlier, at a relatively low pressure, the diffraction peaks for the quartz aggregate
485 started to broaden asymmetrically. As pressure increases, such asymmetry becomes increasingly
486 more significant. Effectively, how the peak shape evolves demonstrates great similarity to that
487 reported for diamond powder under cold compression[40]. High strength granular materials can
488 support a large load on a portion of the grains, while the rest of the grains support a relatively
489 small number of loads, or at any rate support lower normal stresses in certain directions. A
490 conspicuous feature shown in **Figure 8** is that the low-energy sides of both the axial and
491 transverse quartz aggregate peaks shift by a very small amount relative to the larger shifts
492 observed for the high-energy sides. This implies that considerable amount of the grains remains
493 stress-free in both directions. This can occur only if there are significant number of grains with at
494 least a part of their surface area bounded by voids supporting zero pressure, even at the highest
495 applied pressure in this experiment.
496

497 **FIGURE AND TABLE LEGENDS:**
498

499 **Figure 1. A horizontal white X-ray beam is projected through the sample assembly,**
500 **perpendicular to the cylindrical axis of the cell**. The intensity of the diffracted beam X-ray beam
501 is determined by not just one, but an array of 10 detectors distributed along a fixed circle at
502 azimuthal angles of 0°, 22.5°, 45°, 67.5°, 90°, 112.5°, 135°, 157.5°, 180°, and 270° (Only detectors
503 1, 5, 9, and 10 are indicated in this diagram, which are the detectors on which our analysis is
504 based on). These detectors allow the quantification of how stress varies in different orientations.
505 This figure has been modified from Burnley and Zhang[2], Burnley[3], and Cheung et al.[6]
506

507 **Figure 2: Sample Preparation.** (**a**) Core drilling using a rotatory tool with the rotatory
508 workstation package setup as a coring drill press. (**b**) Surface grinding of the end surface of the
509 core sample with a grinding jig (a metal cylinder with a drilled hole).
510

511 **Figure 3: D-DIA cell assembly parts and schematic diagram of cell assembly.** (**a**) A set of D-DIA
512 cell assembly with individual components: cell assembly cube (6.18 mm edge length), boron
513 nitrite sleeve, two alumina rods (diameter of 1.5 mm, height of 1.46 mm), two alumina rings, and
514 two graphite rings. Note: 25-cent coin for scale. (**b**) A schematic diagram inside a cell assembly
515 cube. Note that the tantalum foil is shown in a blue color. It consists of one piece folded in a "U"
516 shape and another two linear pieces separating the cell components. This figure has been
517 modified from Cheung et al.[6]
518

519 **Figure 4: Sample assembly placed in the center of the anvils driven inward simultaneously by**
520 **two wedged guide blocks within a 250 ton hydraulic press at 6-BM-B hutch.** (**a**) The sample
521 assembly is compressed by the anvils driven simultaneously by a wedged guide block pressurized
522 by the hydraulic press. A spacer is inserted to fill up the gaps in the press after the safety latch is
523 removed. (**b**) The schematic diagram shows a side view of a cube-shaped sample assembly

524 (shaded in grey), which is at the center, to be compressed by a set of four, X-ray transparent,
525 sintered diamond, and two tungsten carbide (top/bottom) anvils.

526

527 **Figure 5: The layout of a pump motor controller module, commercial software package, and**
528 **codes for instrument control and data acquisition, and radiography at the end station of 6-BM-**
529 **B.** During the compression experiment, first use the pump motor controller module to close any
530 large gaps between the anvils and the press. Then switch to the software interface for controlling
531 using the hydraulic pump. Both can be aided by visually observing the radiograph captured by a
532 camera.

533

534 **Figure 6: "SAM-85 Press Load Control" window [screenshot].** After switching to the software
535 interface, set the target load to 50 ton in the "SAM-85 Press Load Control" window. Turn the
536 feedback on, with the upper limit of the speed control set to 7 (slowest compression possible)
537 (highlighted in orange).

538

539 **Figure 7: "Diffraction-Imaging-Scan-Prosilica" window screenshot**. Set up an automatic data
540 collection by defining the desired locations of the core (*e.g.,* Press X = 20.738 mm, Press Y = 4.3
541 mm) and aggregate (*e.g.,* Press X = 20.738 mm, Press Y = 4.8 mm) for diffraction (with preset
542 exposure times of 500 s) and X-radiographic imaging.

543

544 **Figure 8: Evolution of the [101] peak for solid grains within quartz aggregate ("quartz agg.")**
545 **(blue) peaks at selected pressures against the crystallites within the novaculite peak (red) at**
546 **zero pressure**. Both axial (left column) and transverse (right column) directions (experiment
547 SIO2_55) are shown for comparison. This figure has been modified from Cheung *et al.*[6]

548

549 **Figure 9: Differential stress.** Differential stress, determined by using the peak broadening
550 method (E×W$_S$/d), for both the solid grains within the quartz aggregate and the crystallites within
551 the novaculite as a function of pressure. The error bars, calculated using standard deviation, are
552 also plotted as reference. Each data point is the result of an average between [101] and [112]
553 peaks. This figure has been modified from Cheung *et al.*[6]

554

555 **DISCUSSION:**
556 We present the detailed procedure for carrying out XRD experiments using the multi-anvil cell at
557 6-BM-B. Perhaps the most critical, and yet most challenging, steps in the above protocol involve
558 optimizing the quality of the sample. Such importance on sample quality applies to almost all
559 rock and mineral deformation experiments. Firstly, it is critical for the end surface of the rock
560 cores to be flat, with both ends parallel to each other and at the same time, perpendicular to the
561 cylindrical surface. That will ensure the external force applied through the anvils is distributed
562 more evenly through the entire end surface of the sample. Other than the end surfaces, the
563 outline of the cylindrical surface attained by the sample is also important because of the
564 geometric assumption in the sample volume calculation.

565

566 As highlighted in a note in Section 1, it is important to reemphasize that the presented method
567 is certainly not the only protocol to prepare good quality samples and other equipment can be

568 used to obtain similar quality. Such flexibility in protocol is also applicable to cell assembly
569 preparation (Section 2). In fact, numerous practical or creative modifications can be applied. For
570 example, many components within the cell assembly (*e.g.,* tantalum) can be substituted with
571 similar materials of lower cost. Moreover, modification can be made depending on the aim of
572 the experiment. For instance, the presented method can be extended to incorporate increased
573 temperature. The experimental procedure (Section 3) can be modified depending on the desired
574 hypothesis, parameter (*e.g.,* ultrasonic wave propagation[44,45]), and data quality (*e.g.,* XRD
575 collection time). In general, the experimental procedure is straightforward; however, a note on
576 troubleshooting is discussed here for successful experimentation. Although data collection is
577 automated during compression, it is advised to plot the XRD data regularly to ensure that the
578 data collection is occurring at the desired location. An explanation for why the phase of the XRD
579 data changes abruptly, is that as the compression progresses, the sample may have shifted
580 upwards (Section 3.1.10) and away from the original location. Instead of the sample itself, the
581 XRD collected is diffracted from the foil or other components of the cell assemblies. In this case,
582 new desired locations for XRD data collection should be updated accordingly (see Section 3.1.10).
583 If this is not the case, it is likely that the phase of the sample has been transited.
584
585 The main limitation of the method presented here is that XRD signals are optimal for samples
586 with fine grain sizes. The X-ray size is limited by front-end slits, which is usually 100 x 100 μm^2.
587 When grain size is as large as 100 μm, the diffraction pattern may become a single crystal
588 diffraction, which will appear as a single peak in the data collection: this loses the desired
589 resolution for the experiment. Many natural detrital sedimentary rocks have grain sizes that are
590 significantly larger than this narrow range. For example, sandstone, by definition, has a grain size
591 ranging from 62.5 to 2,000 μm: hence, besides transmitting only a poor XRD signal, the limited
592 volume of the measurement cell means that it may be impossible to accommodate a
593 representative sized sample of such materials. Unless the sample of interest naturally has an
594 average grain size within the optimal range (*e.g.,* siltstone), the only testing option may be to
595 grind the test material into a mineral aggregate, following the protocol described in Section 1.2,
596 rather than drilling a rock core. In this way, the resulting XRD signal is resolved optimally, but the
597 test material is reduced to a non-cohesive aggregate and its grain size is reduced. Another
598 limitation to this protocol is also closely related to the grain size of the sample. To determine the
599 microstress (differential stress) distribution in the sample using FWHM of the diffraction peak,
600 Gerward *et al.*[11] reported that the total observed FWHM (W_O) is a composite of peak broadening
601 due to strain, grain size, and the instrument:

602

$$W_o{}^2 = W_s{}^2 + W_d{}^2 + W_i{}^2$$

604
605 where the subscript s refers to strain, d to the grain size, and i to the instrument. After subtraction
606 of the peak broadening due to the instrument ($W_i{}^2$), known from the background spectrum
607 obtained in Section 3.1.1, the peak broadening due to strain ($W_S{}^2$) is equal to the observed peak
608 broadening ($W_O{}^2$) minus the peak broadening due to grain size ($W_d{}^2$). However, Weidner[41] noted
609 that unless a significant fraction of grains is smaller than 100 nm, the effect of grain size would
610 not be detected by the energy dispersive detector. Hence, it is worthwhile to measure the
611 postmortem grain size using the scanning electron microscope. Alternatively, it could also be

612 confirmed by comparing the XRD peak width before and after loading.

613

614 The advantage of using the method above over other methodologies is that it can provide the
615 quantification of how stress is distributed in different orientations within a geomaterial. The
616 stress within the sample is measured indirectly by using the atomic lattice spacing within
617 individual grains as a measure of the local elastic strain. Such an approach is fundamentally
618 different from previous compaction studies. In conventional compaction studies, a cylindrical
619 sample is compressed by an axial force across the cross-sectional area. The applied stress
620 magnitude is then estimated simply by dividing the axial force (measured by a load cell) by the
621 initial cross-sectional area. It should be noted, however, that the applied stress magnitude
622 measured in this way is merely an average, bulk value and, as such, does not realistically
623 represent how the local stress state varies within a complex, heterogeneous, granular material.

624

625 Compaction study using the above presented method allows successful quantification of the
626 stress distribution within geomaterials, which ultimately reveals details about the process of
627 compaction. Such knowledge has great importance in application to rock mechanics,
628 geotechnical engineering, mineral physics, and material science. For future directions and
629 applications on rock mechanics and mineral physics experimental investigation, it will be
630 extremely useful to develop and incorporate a pore fluid system into the current setup. There
631 are previous reports of the presence of free water percolating in the Earth's crust down to depths
632 of more than 20 km in depth[10,24]. The presence of a pressurized pore fluid in porous samples
633 would enable better simulation of realistic conditions at depth in the crust, and therefore enable
634 better predictions of mechanical properties and stability. Moreover, recent research[29] indicated
635 that fluid flow in porous media is not as stable as previously suggested by Darcy's Law. This opens
636 up an exciting new direction in investigating how pore fluids permeate through geo-materials in
637 anisotropic and inhomogeneous ways. Moreover, incorporating pore pressure, into the setup
638 would allow simulation of hydraulic fracturing experiments using XRD; an important and timely
639 application to the current increased interest in shale gas production. Instead of 2-D radiography,
640 these future applications would be best aided with an image visualization using 3-D X-ray
641 tomography. These suggested future directions are encapsulated within plans for a new multi-
642 anvil cell currently under installation at the National Synchrotron Light Source II (NSLS-II) X-ray
643 Power Diffraction (XPD) beamline at Brookhaven National Laboratory (BNL).

644

anvil cell assembly development project. All the data files are available from the authors upon request (scheung9@wisc.edu). The samples and data are archived at Mineral Physics Institute at Stony Brook University.

REFERENCES:
1.   Bjørlykke K. Relationships between depositional environments, burial history and rock properties. Some principal aspects of diagenetic processes in sedimentary basins. *Sedimentary Geology*. **301**, 1-14 (2014).
2.   Burnley, P.C., Zhang, D. Interpreting in situ X-ray diffraction data from high pressure deformation experiments using elastic-plastic self-consistent models: An experiment using quartz. *J. Phys. Condens. Matter Solid Earth*. **20** (28), 285201 (2008).
3.   Burnley, P.C. Elastic plastic self-consistent (EPSC) modeling of plastic deformation of fayalite olivine. *American Mineralogist*. **100** (7), 1424-1433 (2015).
4.   Chen, J., Li, L., Weidner, D.J., Vaughan, M.T. Deformation experiments using synchrotron X-rays: in situ stress and strain measurements at high pressure and temperature. *Phys. of the Earth and Planetary Interiors*. **143**, 347-356 (2004).
5.   Cheung, S.N.C. Experimental deformation in sandstone, carbonates, and quartz aggregate. Ph.D. Thesis, *State University of New York at Stony Brook* (2015).
6.   Cheung, S.N.C. *et al*. Stress distribution during cold compression of a quartz aggregate using synchrotron X-ray diffraction: observed yielding, damage, and grain crushing. *J. Geophys. Res. Solid Earth*. **122**, 2724-2735 (2017).
7.   Croizé, D., Ehrenberg, S.N., Bjørlykke, K., Renard, F., Jahren, J. Petrophysical properties of bioclastic platform carbonates: implications for porosity controls during burial. *Marine and Petroleum Geology*. **27** (8), 1765-1774.
8.   Doornhof, D., Kristiansen, T.G., Nagel, N.B., Pattillo, P.D., Sayers, C. Compaction and subsidence. *Oilfield rev.*, **18** (3), 50-68 (2006).
9.   Durham, W.B., Weidner, D.J., Karato, S. New developments in deformation experiments at high pressure. *Rev. Mineral. Geochem*. **51** (1), 22-49 (2002).
10.   Fyfe, W.S. The evolution of the Earth's crust: modern plate tectonics to ancient hot spot tectonics? *Chemical Geology*. **23**(1-4), 89-114 (1978).
11.   Gerward, L., Mo S., Topso, H. Particle size and strain broadening in energy-dispersive –ray powder patters. *J. Appl. Phys*. **47** (3), 822-825 (1976).
12.   Heap, M.J., Farquharson, J.I., Baud, P., Lavallée, Y., Reuschlé, T. Fracture and compaction of andesite in a volcanic edifice. *Bulletin of volcanology*, **77** (6), 55 (2015).
13.   Lavina, B., Dera, P., Downs, R.T. Modern X-ray diffraction methods in mineralogy and geosci. *Reviews in Mineralogy and Geochemistry*. **78** (1), 1-31 (2014).
14.   Leinenweber, K.D. *et al*. Cell assemblies for reproducible multi-anvil experiments (the COMPRES assemblies). *American Mineralogist*. **97**(2-3), 353-368 (2012).
15.   Li, L., Weidner, D.J., Raterron, P., Chen, J., Vaughan, M.T. Stress measurements of deforming olivine at high pressure. *Phys. of the Earth and Planetary Interiors*. **143**, 357-367 (2004).

700   16.   Li, L., Weidner, D.J., Chen, J., Vaughan, M.T., Davis, M., Durham, W.B. X-ray strain analysis
701   at high pressure: Effect of plastic deformation in MgO. *J. App. Phys*. **95** (12), 8357-8365 (2004).
702   17.   Minkoff, S.E., Stone C.M., Bryant S., Peszynska, M., Wheeler, M.F. Coupled fluid flow and
703   geomechanical deformation modeling. *J. Petroleum Sci. and Engineering*. **38** (1), 37-56 (2003).
704   18.   Miyagi, L. *et al*. Deformation and texture development in CalrO 3 post-perovskite phase
705   up to 6 GPa and 1300 K, *Earth and Planetary Sc. Letters*. **268** (3), 515-525 (2008).
706   19.   Morton, R.A., Bernier, J.C., Barras J.A. Evidence of regional subsidence and associated
707   interior wetland loss induced by hydrocarbon production, Gulf Coast region, USA. *Environmental
708   Geology*. **50** (2), 261 (2006).
709   20.   Nagel, N.B. Compaction and subsidence issues within the petroleum industry: From
710   Wilmington to Ekofisk and beyond. *Phys. And Chem. of the Earth, Part A: Solid Earth and Geodesy*.
711   **26** (1-2), 3-14 (2001).
712   21.   Nichols, G. Sedimentology and Stratigraphy. *John Wiley & Sons* (2009).
713   22.   Nicolas, A., Fortin, J., Regnet, J.B., Dimanov, A., Guéguen, Y., Brittle and semi-brittle
714   behaviours of a carbonate rock: influence of water and temperature. *Geophysical Journal
715   International*. **206** (1), 438-456 (2016).
716   23.   Nishiyama, N., Wang, Y., Sanehira, T., Irifune, T., Rivers, M.L. Development of the multi-
717   anvil assembly 6-6 for DIA and DDIA type high-pressure apparatuses. *High Pressure Research*.
718   **28** (3), 307-314 (2008).
719   24.   Nur, A., Walder, J. Time-dependent hydraulics of the Earth's crust. *The role of fluids in
720   crustal processes*. 113-127 (1990).
721   25.   Paterson, M.S. Rock deformation experimentation. The brittle-ductile transition in rocks.
722   The Heard Volume. *The American Geophysical Union, Geophys. Monograph*. **56**, 187-194 (1990).
723   26.   Peng, S.D. Stresses within elastic circular cylinders loaded uniaxially and triaxially. *Int. J.
724   Rock Mech. Min. Sci. Geomech. Abst*. **78** (1), 399-432 (1971).
725   27.   Raterron, P., Merkel, S., Holyoke III, C.W., Axial temperature and gradient and stress
726   measurements in the deformation D-DIA cell using alumina pistons. *Rev. of Sci. Instr*. **84** (4),
727   043906 (2013).
728   28.   Raghavan, R., Chin, L.Y. Productivity changes in reservoirs with stress-dependent
729   permeability. In SPE Annual Technical Conference and Exhibition. *Soc. of Petroleum Engineers*
730   (2002).
731   29.   Reynolds, C.A., Menke, H., Andrew, M., Blunt, M.J., Samuel, K. Dynamic fluid connectivity
732   during steady-state multiphase flow in a sandstone. *Proceedings of National Academy of Sci*. **114**
733   (31), 8187-8192 (2017).
734   30.   Scholle, P. A. A color illustrated guide to constituents, textures, cements, and porosities
735   of sandstones and associated rocks. *AAPG Memoir* No 552.5 SCH (1979).
736   31.   Scholle, P.A., Ulmer-Scholle, D.S. A Color Guide to the Petrography of Carbonate Rocks:
737   Grains, Textures, Porosity, Diagenesis*. AAPG Memoir* **77** (2003).
738   32.   Scholz, C.H. Experimental study of the fracturing process in brittle rock. *J. Geophys. Res*.
739   **73** (4), 1447-1454 (1968).
740   33.   Schutjens, P.M.T.M. *et al*. Compaction-induced porosity/permeability reduction in
741   sandstone reservoirs: Data and model for elasticity-dominated deformation. *SPE Reservoir
742   Evaluation & Engineering*. **7** (3), 202-216 (2004).
743   34.   Simmons, G., and Wang, H. Single Crystal Elastic Constants and Calculated Aggregate

744   Properties. *MIT Press*. Cambridge, MA, 135-160 (1971).

745   35.   Singh, A.K., Balasingh, C., Mao, H.K., Hemley, R.J., Shu, J. Analysis of lattice strains
746   measured under nonhydrostatic pressure. *J. Applied physics*. **83** (12), 7567-7575 (1998).

747   36.   Terzaghi, K.V. Die berechnung der durchlassigkeitsziffer des tones aus dem verlauf der
748   hydrodynamischen spanningsercheinungen. *Sitzungsberichte der Akademie der Wissenschften in*
749   *Wein. Mathematisch-Naturwissenschaftliche Klasse. Abteilung lla*. **132**, 125-138 (1923).

750   37.   Wang, Y., Durham, W.B., Getting, I.C., Weidner, D.J. The deformation D-DIA: a new
751   apparatus for high temperature triaxial deformation to pressures up to 15 GPa. *Rev. Sci. Instrum*.
752   **74** (6), 3002-3011 (2003).

753   38.   Wang, Y., Hilairet, N., Dera, P. Recent advances in high pressure and temperature
754   rheological studies. *J. Earth Sci*. **21** (5), 495-516 (2010).

755   39.   Weidner, D.J. *et al*. Characterisation of Stress, Pressure, and Temperature in SAM85, a
756   DIA Type High Pressure Apparatus. *Geophys. Monogr. Ser. AGU*. Washington, D.C., 13-17 (1992).

757   40.   Weidner, D.J., Wang, Y., Vaughan, M.T. Strength of diamond. *Sci*. **266** (5184), 419-422
758   (1994).

759   41.   Weidner, D.J. Rheological studies at high pressure. *Rev. in Mineralogy and Geochemistry*.
760   **37** (1), 493-524 (1998a).

761   42.   Weidner, D.J., Wang, Y., Chen, G., Vaughan, M.T. Rheology measurements at high
762   pressure and temperature. *Properties of Earth and Planetary Materials at High Pressure and*
763   *Temperature. AGU*. Washington, D.C., 473-482 (1998b).
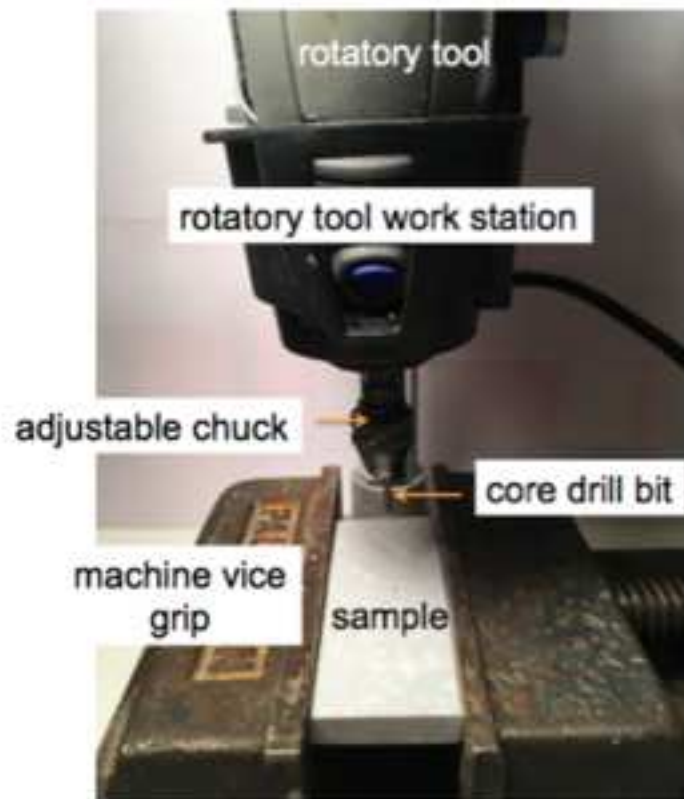
764   43.   Weidner, D.J., Vaughan, M.T., Wang, L., Long, H., Li, L., Dixon, N.A., Durham, W.B. Precise
765   stress measurements with white synchrotron x rays. *Rev. of Sci. Instrum*. **81** (1), 013903 (2010).

766   44.   Weidner, D.J., Li, L., Whitaker, M., Triplett, R. Ultrasonic Acoustic Velocities During Partial
767   Melting of a Mantle Peridotite KLB-1. *J. Geophys. Res: Solid Earth* (2018).
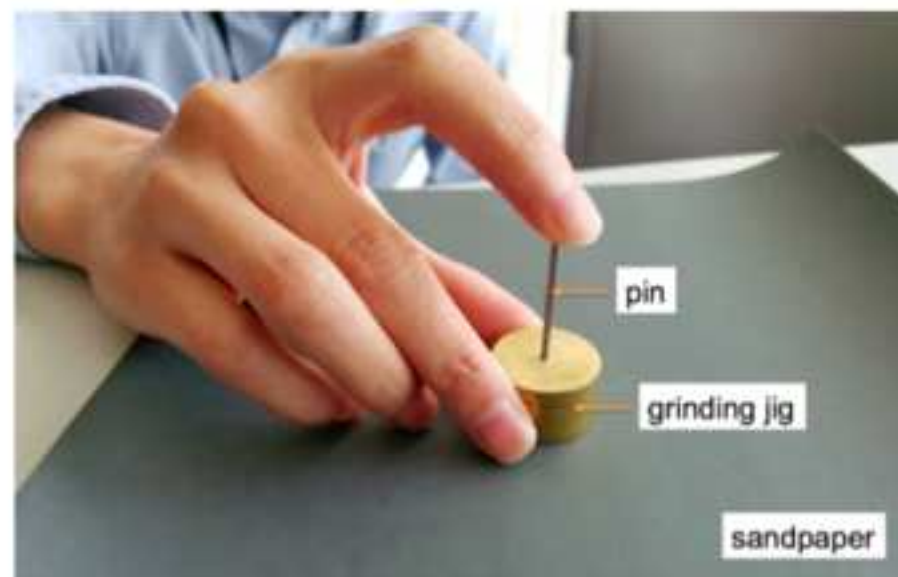
768   45.   Whitaker, M.L., Baldwin, K.J., Huebsch, W.R. DIASCoPE: Directly integrated acoustic
769   system combined with pressure experiments-A new method for fast acoustic velocity
770   measurements at high pressure. *Rev. Sci. Instrum*. **88** (3), 034901 (2017).
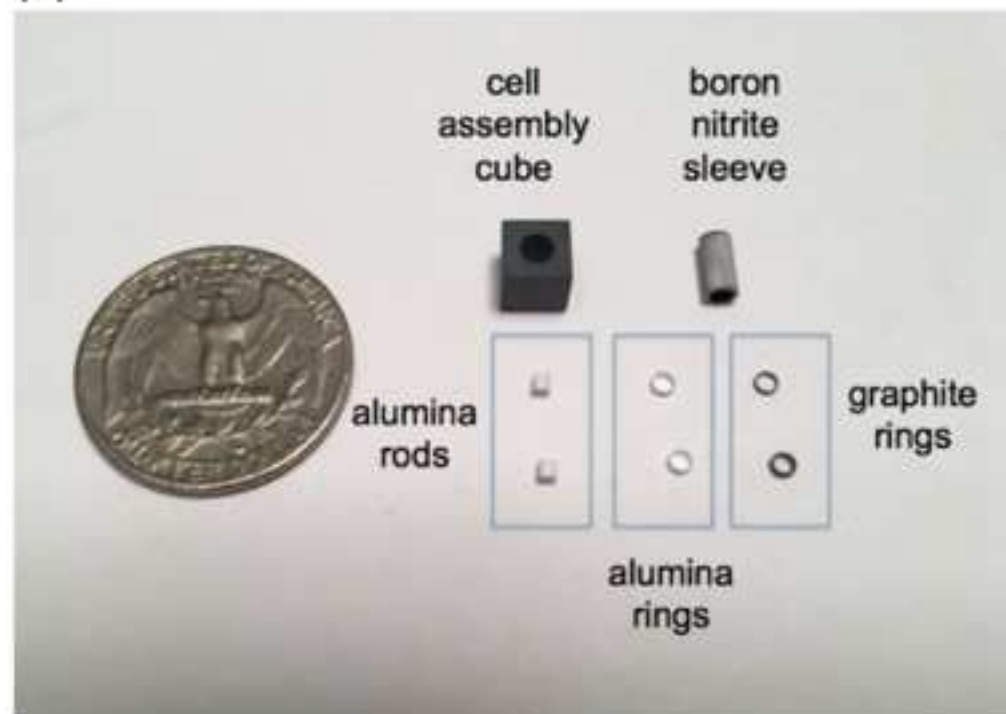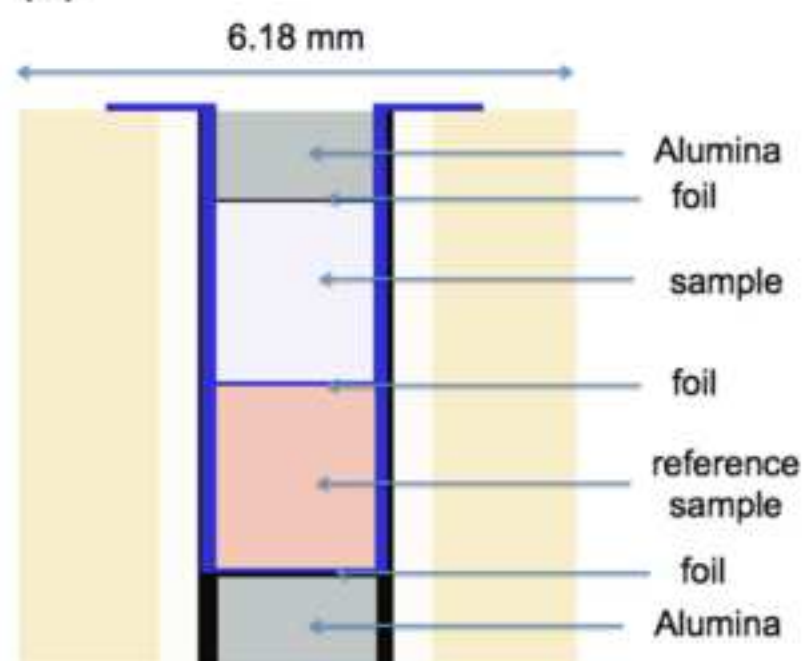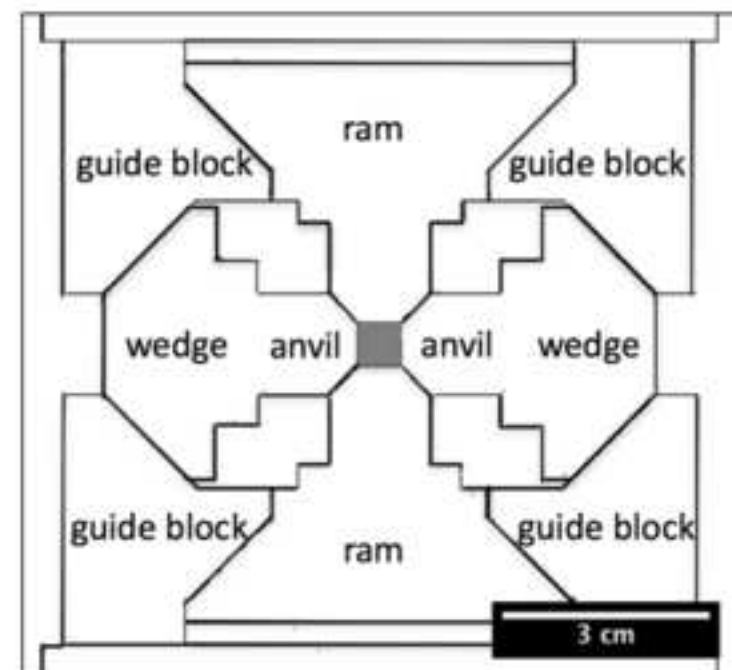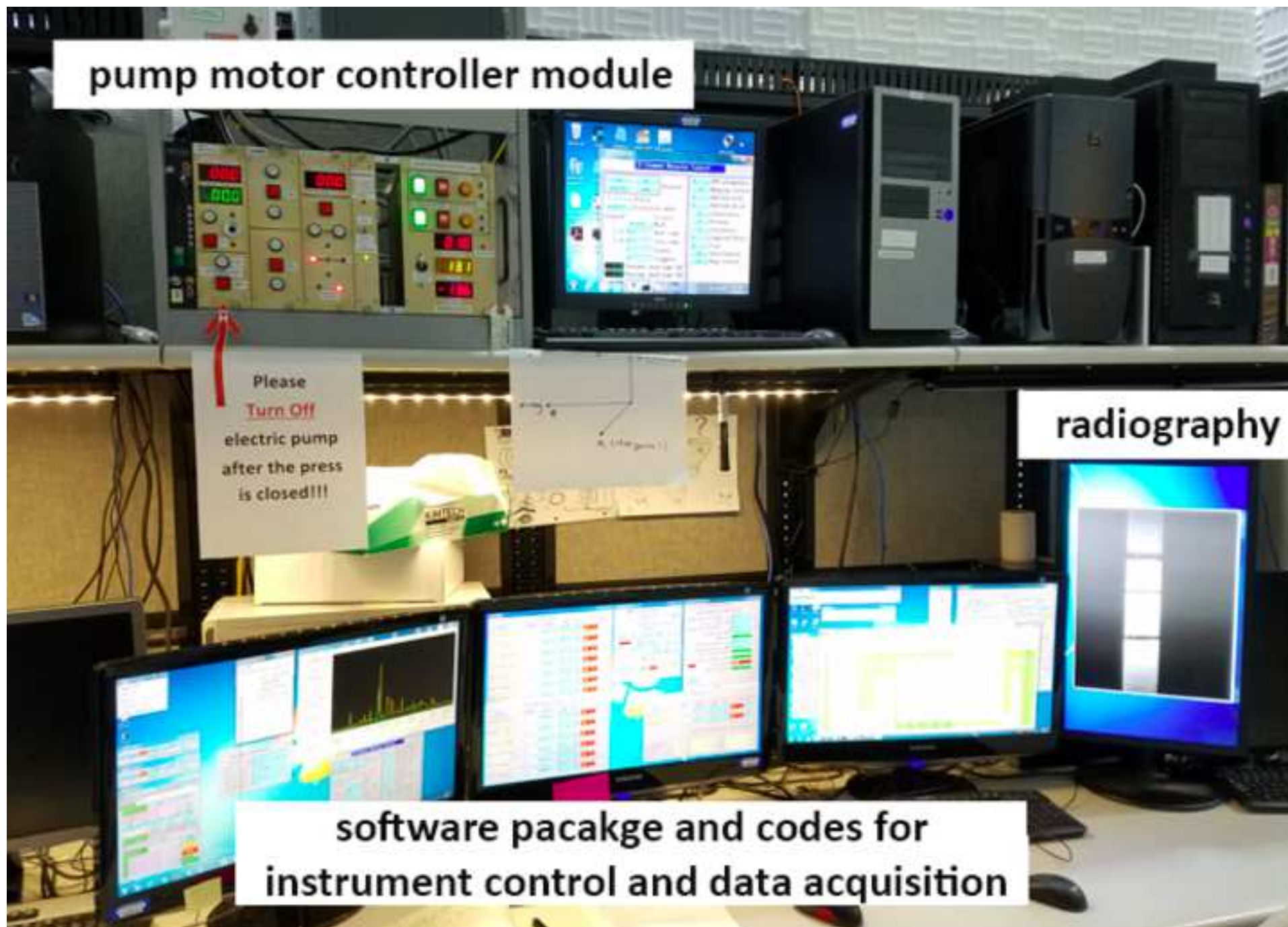
771

772

Figure1

Figure1

Figure2

(a)

rotatory tool

rotatory tool work station

adjustable chuck

core drill bit

machine vice grip

sample

(b)

pin

grinding jig

sandpaper

Figure3

Click here to download Figure Figure3.tiff

(a)

cell assembly cube

boron nitrite sleeve

alumina rods

graphite rings

alumina rings

(b)

6.18 mm

Alumina

foil

sample

foil

reference sample

foil

Alumina

Figure4

(a)

(b)

spacer

sample

X-ray beam in

ram

guide block   guide block

wedge   anvil   anvil   wedge

guide block   guide block

ram

3 cm

Figure5

Figure6

Click here to download Figure Figure6.tiff ⬇

SAM-85 Press Load Control

Load (tons)

0.0

< 50.000 > 1.0 Tweak

Feedback

Plot	On/Off	Rate	Gain
⊡Plot	On ▢	1 second ▢	20.000 (% output/ton error)

Speed control (%)

Stop motor

7.000   < ▭ > 0.000 Tweak

Lower limit -10.000   7.000 Upper limit

Pump Position (% of Maximum) 0.0000

Ramp Load

Final Load (tons)	Time (hours)	Start Ramp	Stop Ramp	Pause Ramp	Resume Ramp
0.000	1.00	Start	Stop	Pause	Resume

Status	Point	Message
Done	0 /1000	
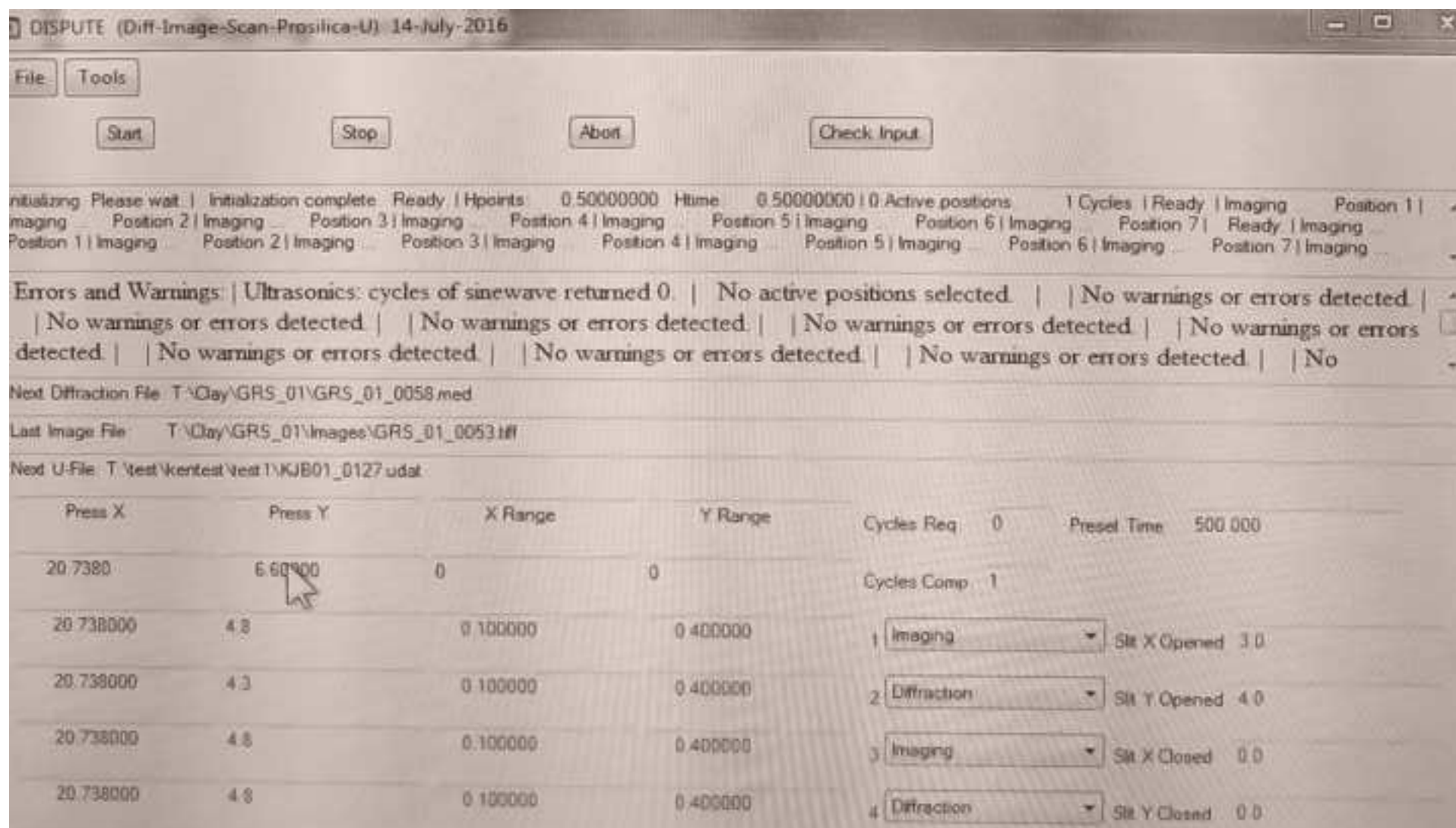
Figure7

Figure7

Figure8

Click here to download Figure Figure8.tiff

Figure9
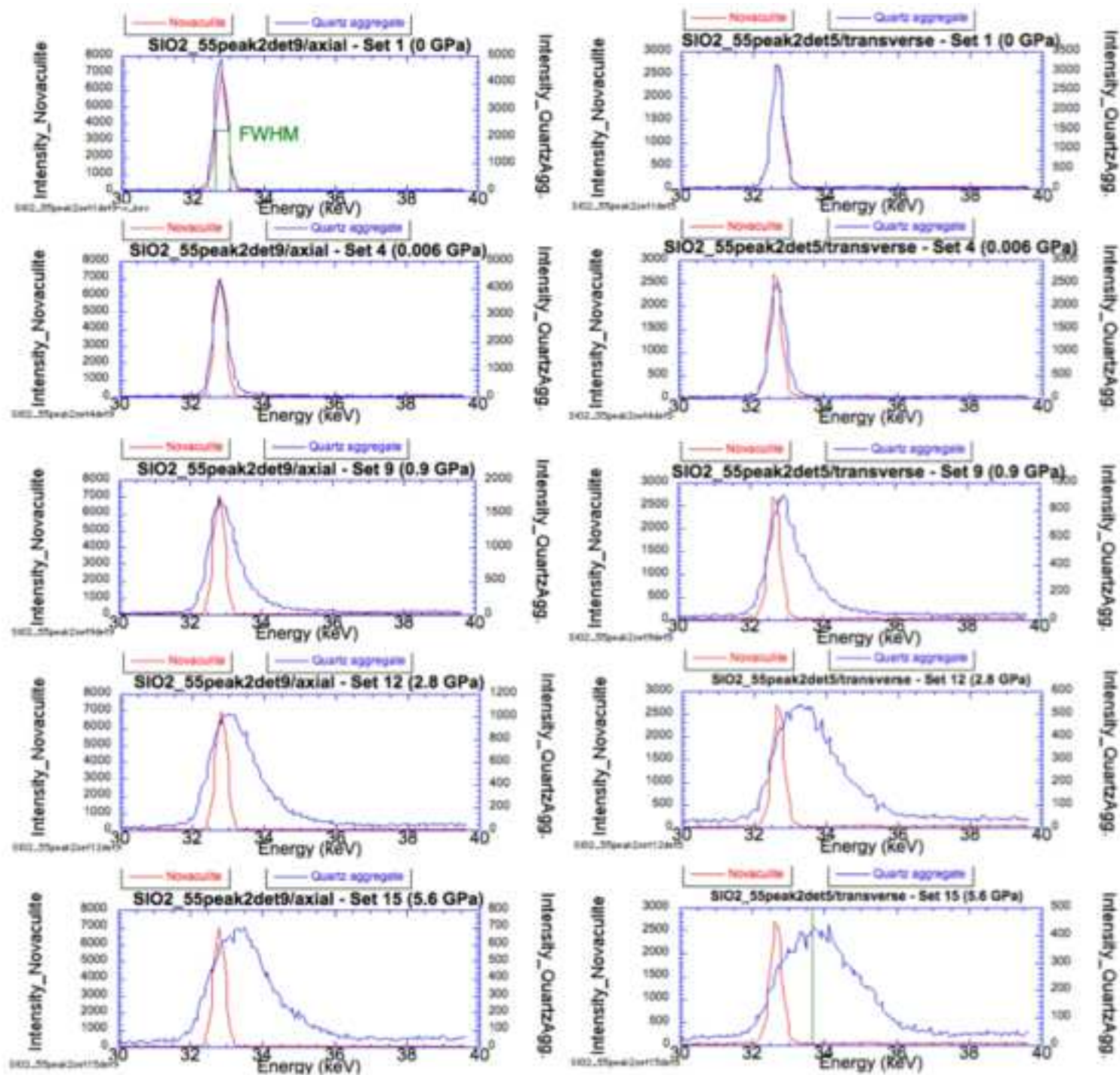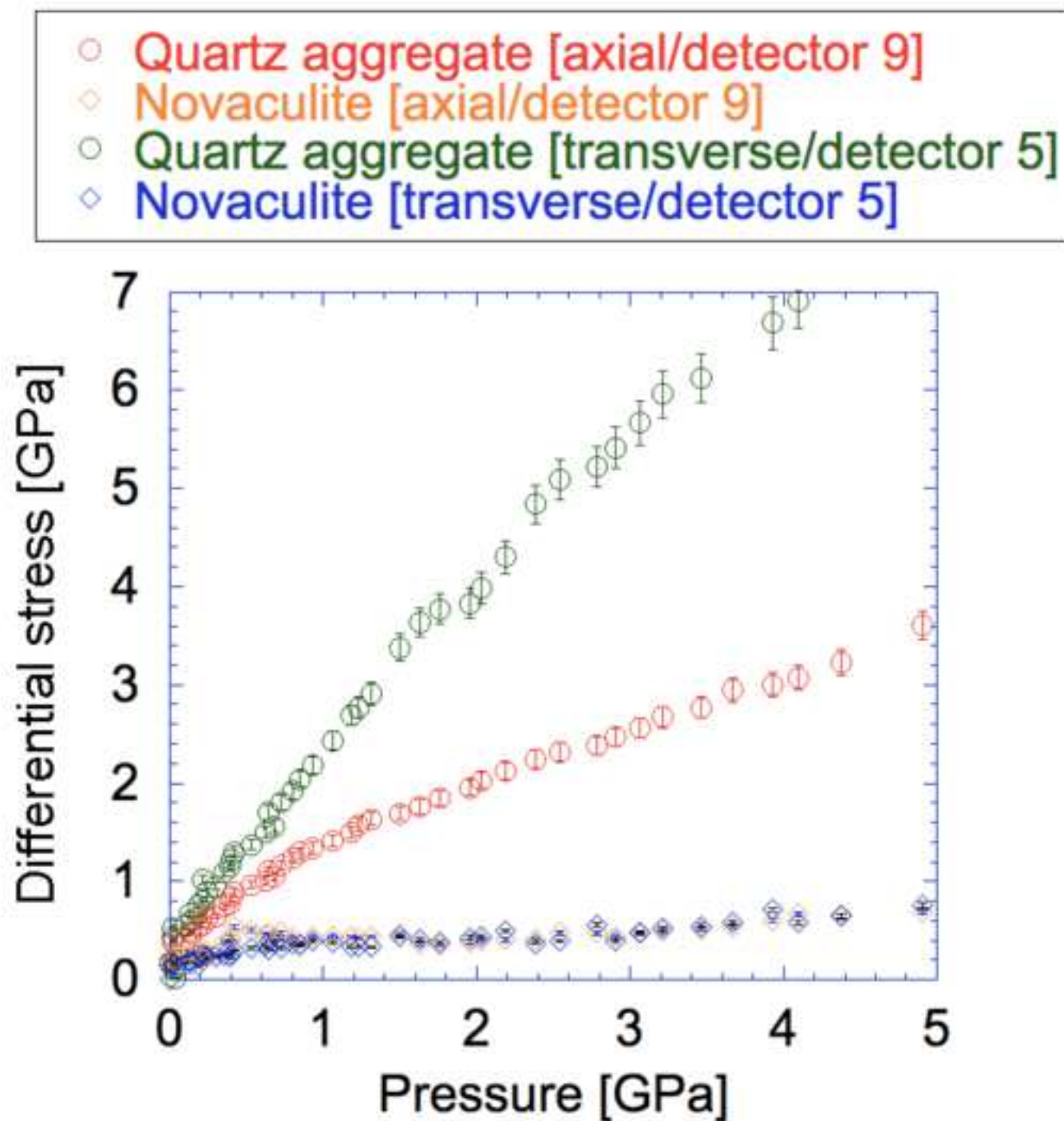
Name of Material/ Equipment	Company	Catalog Number	Comments/Description
Rotatory Tool Workstation Drill Press Work Station with Wrench	Dremel	220-01	
MultiPro Keyless Chuck	Dremel	4486	
Variable-Speed Rotatory Tool	Dremel	4000-6/50	
Super small Diamond Core Drill - 2.5 mm	Dad's Rock Shop	SDCD	
Coolant	NBK	JK-A-NBK-000-020	Grinding Fluid Concentrate US 5 gal / 20 L
commercial software package and codes for instrument control and data acquisition	IDL EPICS and SPEC		installed on the computer at the beamline
CCD Camera	Allied Vision	Prosilica GT	installed at the beamline

jove
JOURNAL OF
VISUALIZED EXPERIMENTS

1 Alewife Center #200
Cambridge, MA 02140
tel. 617.945.9051
www.jove.com

ARTICLE AND VIDEO LICENSE AGREEMENT - UK

Title of Article: Stress distribution during cold compression of rocks and mineral aggregates using X-ray diffraction at 6BM-B

Author(s): Cecilia S N Cheung, Donald J Weidner, Li Li, Philip G Meredith, Haiyan Chen, Matthew L Whitaker, Xianyin Chen

Item 1 (check one box): The Author elects to have the Materials be made available (as described at http://www.jove.com/author) via: ☑ Standard Access ☐ Open Access

Item 2 (check one box):

☑ The Author is NOT a United States government employee.

☐ The Author is a United States government employee and the Materials were prepared in the course of his or her duties as a United States government employee.

☐ The Author is a United States government employee but the Materials were NOT prepared in the course of his or her duties as a United States government employee.

ARTICLE AND VIDEO LICENSE AGREEMENT

1. <u>Defined Terms.</u> As used in this Article and Video License Agreement, the following terms shall have the following meanings: "**Agreement**" means this Article and Video License Agreement; "**Article**" means the article specified on the last page of this Agreement, including any associated materials such as texts, figures, tables, artwork, abstracts, or summaries contained therein; "**Author**" means the author who is a signatory to this Agreement; "**Collective Work**" means a work, such as a periodical issue, anthology or encyclopedia, in which the Materials in their entirety in unmodified form, along with a number of other contributions, constituting separate and independent works in themselves, are assembled into a collective whole; "**CRC License**" means the Creative Commons Attribution 3.0 Agreement (also known as CC-BY), the terms and conditions of which can be found at: http://creativecommons.org/licenses/by/3.0/us/legalcode; "**Derivative Work**" means a work based upon the Materials or upon the Materials and other pre-existing works, such as a translation, musical arrangement, dramatization, fictionalization, motion picture version, sound recording, art reproduction, abridgment, condensation, or any other form in which the Materials may be recast, transformed, or adapted; "**Institution**" means the institution, listed on the last page of this Agreement, by which the Author was employed at the time of the creation of the Materials; "**JoVE**" means MyJove Corporation, a Massachusetts corporation and the publisher of *The Journal of Visualized Experiments*;

"**Materials**" means the Article and / or the Video; "**Parties**" means the Author and JoVE; "**Video**" means any video(s) made by the Author, alone or in conjunction with any other parties, or by JoVE or its affiliates or agents, individually or in collaboration with the Author or any other parties, incorporating all or any portion of the Article, and in which the Author may or may not appear.

2. <u>Background.</u> The Author, who is the author of the Article, in order to ensure the dissemination and protection of the Article, desires to have the JoVE publish the Article and create and transmit videos based on the Article. In furtherance of such goals, the Parties desire to memorialize in this Agreement the respective rights of each Party in and to the Article and the Video.

3. <u>Grant of Rights in Article.</u> In consideration of JoVE agreeing to publish the Article, the Author hereby grants to JoVE, subject to **Sections 4** and **7** below, the exclusive, royalty-free, perpetual (for the full term of copyright in the Article, including any extensions thereto) license (a) to publish, reproduce, distribute, display and store the Article in all forms, formats and media whether now known or hereafter developed (including without limitation in print, digital and electronic form) throughout the world, (b) to translate the Article into other languages, create adaptations, summaries or extracts of the Article or other Derivative Works (including, without limitation, the Video) or Collective Works based on all or any portion of the Article and exercise all of the rights set forth in (a) above in such translations, adaptations, summaries, extracts, Derivative Works or Collective Works and

(c) to license others to do any or all of the above. The foregoing rights may be exercised in all media and formats, whether now known or hereafter devised, and include the right to make such modifications as are technically necessary to exercise the rights in other media and formats. If the "Open Access" box has been checked in **Item 1** above, JoVE and the Author hereby grant to the public all such rights in the Article as provided in, but subject to all limitations and requirements set forth in, the CRC License.

4. <u>Retention of Rights in Article.</u> Notwithstanding the exclusive license granted to JoVE in **Section 3** above, the

Author shall, with respect to the Article, retain the non-exclusive right to use all or part of the Article for the non-commercial purpose of giving lectures, presentations or teaching classes, and to post a copy of the Article on the

Institution's website or the Author's personal website, in each case provided that a link to the Article on the JoVE website is provided and notice of JoVE's copyright in the Article is included. All non-copyright intellectual property rights in and to the Article, such as patent rights, shall remain with the Author.

5. Grant of Rights in Video – Standard Access. This Section 5 applies if the "Standard Access" box has been checked in Item 1 above or if no box has been checked in Item 1 above. In consideration of JoVE agreeing to produce, display or otherwise assist with the Video, the Author hereby acknowledges and agrees that, Subject to Section 7 below, JoVE is and shall be the sole and exclusive owner of all rights of any nature, including, without limitation, all copyrights, in and to the Video. To the extent that, by law, the Author is deemed, now or at any time in the future, to have any rights of any nature in or to the Video, the Author hereby disclaims all such rights and transfers all such rights to JoVE.

6. Grant of Rights in Video – Open Access. This Section 6 applies only if the "Open Access" box has been checked in Item 1 above. In consideration of JoVE agreeing to produce, display or otherwise assist with the Video, the Author hereby grants to JoVE, subject to Section 7 below, the exclusive, royalty-free, perpetual (for the full term of copyright in the Article, including any extensions thereto) license (a) to publish, reproduce, distribute, display and store the Video in all forms, formats and media whether now known or hereafter developed (including without limitation in print, digital and electronic form) throughout the world, (b) to translate the Video into other languages, create adaptations, summaries or extracts of the Video or other Derivative Works or Collective Works based on all or any portion of the Video and exercise all of the rights set forth in (a) above in such translations, adaptations, summaries, extracts, Derivative Works or Collective Works and (c) to license others to do any or all of the above. The foregoing rights may be exercised in all media and formats, whether now known or hereafter devised, and include the right to make such modifications as are technically necessary to exercise the rights in other media and formats.

7. Government Employees. If the Author is a United States government employee and the Article was prepared in the course of his or her duties as a United States government employee, as indicated in Item 2 above, and any of the licenses or grants granted by the Author hereunder exceed the scope of the 17 U.S.C. 403, then the rights granted hereunder shall be limited to the maximum rights permitted under such statute. In such case, all provisions contained herein that are not in conflict with such statute shall remain in full force and effect, and all provisions contained herein that do so conflict

shall be deemed to be amended so as to provide to JoVE the maximum rights permissible within such statute.

8. Likeness, Privacy, Personality. The Author hereby grants JoVE the right to use the Author's name, voice, likeness, picture, photograph, image, biography and performance in any way, commercial or otherwise, in connection with the Materials and the sale, promotion and distribution thereof. The Author hereby waives any and all rights he or she may have, relating to his or her appearance in the Video or otherwise relating to the Materials, under all applicable privacy, likeness, personality or similar laws.

9. Author Warranties. The Author represents and warrants that the Article is original, that it has not been published, that the copyright interest is owned by the Author (or, if more than one author is listed at the beginning of this Agreement, by such authors collectively) and has not been assigned, licensed, or otherwise transferred to any other party. The Author represents and warrants that the author(s) listed at the top of this Agreement are the only authors of the Materials. If more than one author is listed at the top of this Agreement and if any such author has not entered into a separate Article and Video License Agreement with JoVE relating to the Materials, the Author represents and warrants that the Author has been authorized by each of the other such authors to execute this Agreement on his or her behalf and to bind him or her with respect to the terms of this Agreement as if each of them had been a party hereto as an Author. The Author warrants that the use, reproduction, distribution, public or private performance or display, and/or modification of all or any portion of the Materials does not and will not violate, infringe and/or misappropriate the patent, trademark, intellectual property or other rights of any third party. The Author represents and warrants that it has and will continue to comply with all government, institutional and other regulations, including, without limitation all institutional, laboratory, hospital, ethical, human and animal treatment, privacy, and all other rules, regulations, laws, procedures or guidelines, applicable to the Materials, and that all research involving human and animal subjects has been approved by the Author's relevant institutional review board.

10. JoVE Discretion. If the Author requests the assistance of JoVE in producing the Video in the Author's facility, the Author shall ensure that the presence of JoVE employees, agents or independent contractors is in accordance with the relevant regulations of the Author's institution. If more than one author is listed at the beginning of this Agreement, JoVE may, in its sole discretion, elect not take any action with respect to the Article until such time as it has received complete, executed Article and Video License Agreements from each such author. JoVE reserves the right, in its absolute and sole discretion and without giving any reason therefore, to accept or decline any work submitted to JoVE. JoVE and its employees, agents and independent contractors shall have full, unfettered access to the facilities of the Author or of the Author's institution as necessary to make the Video, whether actually published or not. JoVE has sole discretion as to the method of making and publishing the Materials, including,

2

![JoVE logo] JOURNAL OF VISUALIZED EXPERIMENTS

1 Alewife Center #200
Cambridge, MA 02140
tel. 617.945.9051
www.jove.com

ARTICLE AND VIDEO LICENSE AGREEMENT – UK

without limitation, to all decisions regarding editing, lighting, filming, timing of publication, if any, length, quality, content and the like.

11. Indemnification. The Author agrees to indemnify JoVE and/or its successors and assigns from and against any and all claims, costs, and expenses, including attorney's fees, arising out of any breach of any warranty or other representations contained herein. The Author further agrees to indemnify and hold harmless JoVE from and against any and all claims, costs, and expenses, including attorney's fees, resulting from the breach by the Author of any representation or warranty contained herein or from allegations or instances of violation of intellectual property rights, damage to the Author's or the Author's institution's facilities, fraud, libel, defamation, research, equipment, experiments, property damage, personal injury, violations of institutional, laboratory, hospital, ethical, human and animal treatment, privacy or other rules, regulations, laws, procedures or guidelines, liabilities and other losses or damages related in any way to the submission of work to JoVE, making of videos by JoVE, or publication in JoVE or elsewhere by JoVE. The Author shall be responsible for, and shall hold JoVE harmless from, damages caused by lack of sterilization, lack of cleanliness or by contamination due to the making of a video by JoVE its employees, agents or independent contractors. All sterilization, cleanliness or decontamination procedures shall be solely the responsibility of the Author and shall be undertaken at the Author's expense. All indemnifications provided herein shall include JoVE's attorney's fees and costs related to said losses or

damages. Such indemnification and holding harmless shall include such losses or damages incurred by, or in connection with, acts or omissions of JoVE, its employees, agents or independent contractors.

12. Fees. To cover the cost incurred for publication, JoVE must receive payment before production and publication the Materials. Payment is due in 21 days of invoice. Should the Materials not be published due to an editorial or production decision, these funds will be returned to the Author. Withdrawal by the Author of any submitted Materials after final peer review approval will result in a US$1,200 fee to cover pre-production expenses incurred by JoVE. If payment is not received by the completion of filming, production and publication of the Materials will be suspended until payment is received.

13. Transfer, Governing Law. This Agreement may be assigned by JoVE and shall inure to the benefits of any of JoVE's successors and assignees. This Agreement shall be governed and construed by the internal laws of the Commonwealth of Massachusetts without giving effect to any conflict of law provision thereunder. This Agreement may be executed in counterparts, each of which shall be deemed an original, but all of which together shall be deemed to me one and the same agreement. A signed copy of this Agreement delivered by facsimile, e-mail or other means of electronic transmission shall be deemed to have the same legal effect as delivery of an original signed copy of this Agreement.

A signed copy of this document must be sent with all new submissions. Only one Agreement required per submission.

AUTHOR:

Name: Cecilia S N Cheung

Department: Department of Geoscience

Institution: Stony Brook University

Article Title: Stress distribution during cold compression of rocks and mineral aggregates using X-ray diffraction at 6BM-B

Signature: [signature]   Date: 1 0 3 0 2 0 1 7

Please submit a signed and dated copy of this license by one of the following three methods:
1) Upload a scanned copy as a PDF to the JoVE submission site upon manuscript submission (preferred);
2) Fax the document to +1.866.381.2236; or
3) Mail the document to JoVE / Atn: JoVE Editorial / 1 Alewife Center Suite 200 / Cambridge, MA 02140

For questions, please email editorial@jove.com or call +1.617.945.9051.

MS # (internal use):

University of Wisconsin-Madison
Geological Engineering
Engineering Hall
2/16/2018

Dr. Alisha Dsouza
Senior Review Editor
JoVE

Dear Dr. DSouza,

Thank you very much for the latest editorial review on our manuscript, JoVE57555R1 Stress distribution during cold compression of rocks and mineral aggregates using synchrotron based X-ray diffraction. We find the comments useful and have now revised our manuscript based on all the suggestions. We have tracked the changes to highlight all the edits. Below is a line-by-line response that addresses each of the editorial review comments individually.

Line 5: "Please ensure that your funding source allows publication under standard access. Several UK-based governmental funding sources require open access publication."
Thanks for checking in on the type of access on our publication. We decided to keep our article to be under 'standard access' as this research was not funded by a grant or studentship from UK public funding and hence not required to be an open access publication.

Line 125: "Please note that some steps were edited for clarity, and highlighting was modified to meet JoVE requirements. Please verify and approve these minor edits."
Thanks once again for your edits! After verification, we are glad to approve these minor edits.

Line 136: "The length of the protocol section exceeded the 2.75-highlighted page limit. I have unhighlighted 1.3 to meet the length limits."
Thanks for shortening the highlighted section, we gladly accept this change.

Line 210: "It was previously unclear when the grains were suspended in ethanol. Please verify these additions."
"After grinding until the average diameter of the grains is 4 μm" has been added to clarify when the grains were suspended in ethanol.

Line 317: "What is done to analyze? Unclear what we would film here."
The section has been partly rewritten to clarify details on analysis: "Analyze the alumina X-ray diffraction (XRD) pattern, which contains built-in Cobalt-57 (Co-57) fluorescence peaks, by calculating the average peak position (Horiz X, Vert Y and Beam Z dimensions) over the different detectors. Enter the average values as new pedestal positions in the 6motors.adl panel. Recollect a diffraction pattern and save

as an energy dispersive diffraction (EDF) file which constrains the 2-theta angle and the correlation function between detector channel and X-ray energy for each of the 10 detectors." However, we decide that the analysis section should be omitted from filming.

Line 324: "What is done to perform this spectrum collection step? Alternatively, a software screenshot of this will suffice."
"Remove the alumina standard and collect an open press X-ray spectrum by clicking start button on the 12 Element Detector Control Panel" has been added to describe how the spectrum collection step is performed.

Line 341: "Unclear what is done here. Please mention any software button clicks in brief."
It has been rewritten to include buttons needed to be pushed to carry out the protocol.
"In the low-pressure pump panel (labelled as pump motor controller module in Figure 5), turn the "low pressure pump button – on" and push the "up" button next to the "top ram" label to move the top ram to the top against the spacer (Figure 4a)."

Line 349: "Unclear what is done here. Please mention any software button clicks in brief."
Button click has been added for clarification: Move the sample position in Z direction (parallel to the beam) using the "jog" button in the 6motors.adl panel such that the center of the sample in the ImageJ EPICS area detector plugin software panel align with the diffraction focus mark on the screen, to minimize parasitic diffraction and optimize signal to noise ratio.

Line 382, 385: "Unclear what is done here. Please mention any software button clicks in brief."
New button clicks are added to clarify this step: Collect diffraction spectra by clicking the start button on the 12 Element Detector Control Pump for the core and the aggregate ("jog" button along pedestal Z to move between samples) separately, each with an exposure time of 500 s, at ambient conditions. On the NDFileTIFF.adl panel, click "capture-start" button to capture a radiograph (Figure 5) of these samples with an exposure time of ~6 ms.

Line 404, 409: "Unclear what is done here. Please mention any software button clicks in brief."
The section has been rewritten with software button clicks added as follows:
After reaching the target load of 50 ton, click "stop" button to stop the automatic data collection in the **Diffraction-Imaging-Scan-Prosilica** panel (Figure 7). In the **SAM-85 Press Load Control** window, decompress the sample by setting the lower limit of the speed control to -10 and change the target load to 0 ton.

After unloading, collect diffraction spectra by clicking the start button on the 12 Element Detector Control Pump for the core and the aggregate separately each at

exposure time of 500 s. On the NDFileTIFF.adl panel, click "capture-start" button to capture a radiograph (Figure 5) of these samples with an exposure time of ~6 ms.

Line 414, 416: Unclear how this is done, Please describe the step you perform to achieve this.

New software button clicks and new screen shot (Figure 7) are now included: "After unloading, collect diffraction spectra by clicking the "start" button on the 12 Element Detector Control Pump panel for the core and the aggregate separately each at exposure time of 500 s. On the NDFileTIFF.adl panel, click "capture-start" button to capture a radiograph (Figure 5) of these samples with an exposure time of ~6 ms."

Line 419: "Unclear what is done here. Please mention any software button clicks in brief."

New software button clicks and new screen shots are now included: "In the low-pressure pump panel (labelled as pump motor controller module in Figure 5), open the **pressurize valve**. Push the "low pressure pump – on" button, and press the "down" buttons both next to the "top ram" and "bottom ram" labels to move both the top and the bottom ram downwards until the green **Down** light becomes illuminated, then stop driving both rams."

Line 490, 491: "How and where is this done?", "How?"

New button clicks have been included: In the low-pressure pump panel, press the "out" button near the "spacer block" label to move the spacer arm to the "out" position, and then press "up" button near the "top ram" label to drive the top ram up until the safety lock engages. Turn all the controls off in the pump motor controller unit (Figure 5) afterwards. Slowly manually move the lateral anvils outwards and remove the sample assembly.

Line 620: "Please revise grammar"

"Aid" has been corrected to "aided".

Line 620: "Add to the table of materials"

"CCD Camera Prosilica GT by Allied Vision" has been added to the table of materials.

Line 637: "Please label the x and y axes. Please add units for each as well."

New x and y axes with units have been added.

Line 639: "Define the error bars, do these represent standard deviation? Also, how many samples/measurements per point?"

The error bars, calculated using standard deviation, are also plotted as reference. For each data point, it is a result of an average between [101] and [112] peaks.

Line 752: "Please italicize all journal titles"

The journal titles have now been italicized.

Thank you once again for the useful edits and suggestions. I hope the above point to point respond is useful. Feel free to let me know if you have any questions. I look forward to hearing from you.

Best regards,

Cecilia Cheung & co-authors

Click here to download Supplemental File (Figures, Permissions, ⬇
etc.) PermissionJGRSolidEarth.pdf

8/29/17, 10:09 AM

JOHN WILEY AND SONS LICENSE
TERMS AND CONDITIONS

Aug 29, 2017

This Agreement between Dr. Cecilia S. N. Cheung ("You") and John Wiley and Sons ("John Wiley and Sons") consists of your license details and the terms and conditions provided by John Wiley and Sons and Copyright Clearance Center.

License Number	4178260819010
License date	Aug 29, 2017
Licensed Content Publisher	John Wiley and Sons
Licensed Content Publication	Journal of Geophysical Research: Solid Earth
Licensed Content Title	Stress distribution during cold compression of a quartz aggregate using synchrotron X-ray diffraction: Observed yielding, damage, and grain crushing
Licensed Content Author	C. S. N. Cheung,D. J. Weidner,L. Li,P. G. Meredith,H. Chen,M. L. Whitaker,X. Chen
Licensed Content Date	Apr 22, 2017
Licensed Content Pages	12
Type of use	Journal/Magazine
Requestor type	Author of this Wiley article
Is the reuse sponsored by or associated with a pharmaceutical or medical products company?	no
Format	Print and electronic
Portion	Figure/table
Number of figures/tables	3
Original Wiley figure/table number(s)	Figure 1, 6, 7
Will you be translating?	No
Circulation	100
Title of new article	Stress distribution during cold compression of rocks and mineral aggregates using X-ray diffraction at 6BM
Publication the new article is in	Journal of Visualized Experiments
Publisher of new article	Journal of Visualized Experiments
Author of new article	Cecilia S N Cheung, Donald J Weidner, Li Li, Philip G Meredith, Haiyan Chen, Matthew L Whitaker, Xianyin Chen

Expected publication date of new article	Jan 2018
Estimated size of new article (pages)	11
Requestor Location	Dr. Cecilia S. N. Cheung 518 W Main St MADISON, WI 53703 United States Attn: Dr. Cecilia S. N. Cheung
Publisher Tax ID	EU826007151
Billing Type	Invoice
Billing Address	Dr. Cecilia S. N. Cheung 518 W Main St MADISON, WI 53703 United States Attn:
Total	0.00 USD
Terms and Conditions	

TERMS AND CONDITIONS

license. Permission is granted subject to an appropriate acknowledgement given to the author, title of the material/book/journal and the publisher. You shall also duplicate the copyright notice that appears in the Wiley publication in your use of the Wiley Material. Permission is also granted on the understanding that nowhere in the text is a previously published source acknowledged for all or part of this Wiley Material. Any third party content is expressly excluded from this permission.

- With respect to the Wiley Materials, all rights are reserved. Except as expressly granted by the terms of the license, no part of the Wiley Materials may be copied, modified, adapted (except for minor reformatting required by the new Publication), translated, reproduced, transferred or distributed, in any form or by any means, and no derivative works may be made based on the Wiley Materials without the prior permission of the respective copyright owner.**For STM Signatory Publishers clearing permission under the terms of the STM Permissions Guidelines only, the terms of the license are extended to include subsequent editions and for editions in other languages, provided such editions are for the work as a whole in situ and does not involve the separate exploitation of the permitted figures or extracts,** You may not alter, remove or suppress in any manner any copyright, trademark or other notices displayed by the Wiley Materials. You may not license, rent, sell, loan, lease, pledge, offer as security, transfer or assign the Wiley Materials on a stand-alone basis, or any of the rights granted to you hereunder to any other person.

- The Wiley Materials and all of the intellectual property rights therein shall at all times remain the exclusive property of John Wiley & Sons Inc, the Wiley Companies, or their respective licensors, and your interest therein is only that of having possession of and the right to reproduce the Wiley Materials pursuant to Section 2 herein during the continuance of this Agreement. You agree that you own no right, title or interest in or to the Wiley Materials or any of the intellectual property rights therein. You shall have no rights hereunder other than the license as provided for above in Section 2. No right, license or interest to any trademark, trade name, service mark or other branding ("Marks") of WILEY or its licensors is granted hereunder, and you agree that you shall not assert any such right, license or interest with respect thereto

- NEITHER WILEY NOR ITS LICENSORS MAKES ANY WARRANTY OR REPRESENTATION OF ANY KIND TO YOU OR ANY THIRD PARTY, EXPRESS, IMPLIED OR STATUTORY, WITH RESPECT TO THE MATERIALS OR THE ACCURACY OF ANY INFORMATION CONTAINED IN THE MATERIALS, INCLUDING, WITHOUT LIMITATION, ANY IMPLIED WARRANTY OF MERCHANTABILITY, ACCURACY, SATISFACTORY QUALITY, FITNESS FOR A PARTICULAR PURPOSE, USABILITY, INTEGRATION OR NON-INFRINGEMENT AND ALL SUCH WARRANTIES ARE HEREBY EXCLUDED BY WILEY AND ITS LICENSORS AND WAIVED BY YOU.

- WILEY shall have the right to terminate this Agreement immediately upon breach of this Agreement by you.

- You shall indemnify, defend and hold harmless WILEY, its Licensors and their respective directors, officers, agents and employees, from and against any actual or threatened claims, demands, causes of action or proceedings arising from any breach of this Agreement by you.

- IN NO EVENT SHALL WILEY OR ITS LICENSORS BE LIABLE TO YOU OR ANY OTHER PARTY OR ANY OTHER PERSON OR ENTITY FOR ANY SPECIAL, CONSEQUENTIAL, INCIDENTAL, INDIRECT, EXEMPLARY OR PUNITIVE DAMAGES, HOWEVER CAUSED, ARISING OUT OF OR IN CONNECTION WITH THE DOWNLOADING, PROVISIONING, VIEWING OR USE OF THE MATERIALS REGARDLESS OF THE FORM OF ACTION, WHETHER FOR BREACH OF CONTRACT, BREACH OF WARRANTY, TORT, NEGLIGENCE, INFRINGEMENT OR OTHERWISE (INCLUDING, WITHOUT LIMITATION, DAMAGES BASED ON LOSS OF PROFITS, DATA, FILES, USE, BUSINESS OPPORTUNITY OR CLAIMS OF THIRD PARTIES), AND WHETHER OR NOT THE PARTY HAS BEEN ADVISED OF THE POSSIBILITY OF SUCH DAMAGES. THIS LIMITATION SHALL APPLY NOTWITHSTANDING ANY FAILURE OF ESSENTIAL PURPOSE OF ANY LIMITED REMEDY PROVIDED HEREIN.

- Should any provision of this Agreement be held by a court of competent jurisdiction to be illegal, invalid, or unenforceable, that provision shall be deemed amended to achieve as nearly as possible the same economic effect as the original provision, and the legality, validity and enforceability of the remaining provisions of this Agreement shall not be affected or impaired thereby.

- The failure of either party to enforce any term or condition of this Agreement shall not constitute a waiver of either party's right to enforce each and every term and condition of this Agreement. No breach under this agreement shall be deemed waived or excused by either party unless such waiver or consent is in writing signed by the party granting such waiver or consent. The waiver by or consent of a party to a breach of any provision of this Agreement shall not operate or be construed as a waiver of or consent to any other or subsequent breach by such other party.

- This Agreement may not be assigned (including by operation of law or otherwise) by you without WILEY's prior written consent.

- Any fee required for this permission shall be non-refundable after thirty (30) days from receipt by the CCC.

- These terms and conditions together with CCC's Billing and Payment terms and conditions (which are incorporated herein) form the entire agreement between you and WILEY concerning this licensing transaction and (in the absence of fraud) supersedes all prior agreements and representations of the parties, oral or written. This Agreement may not be amended except in writing signed by both parties. This Agreement shall be binding upon and inure to the benefit of the parties' successors, legal representatives, and authorized assigns.

- In the event of any conflict between your obligations established by these terms and conditions and those established by CCC's Billing and Payment terms and conditions, these terms and conditions shall prevail.

- WILEY expressly reserves all rights not specifically granted in the combination of (i) the license details provided by you and accepted in the course of this licensing transaction, (ii) these terms and conditions and (iii) CCC's Billing and Payment terms and conditions.

- This Agreement will be void if the Type of Use, Format, Circulation, or Requestor Type was misrepresented during the licensing process.

- This Agreement shall be governed by and construed in accordance with the laws of the State of New York, USA, without regards to such state's conflict of law rules. Any legal action, suit or proceeding arising out of or relating to these Terms and Conditions or the breach thereof shall be instituted in a court of competent jurisdiction in New York County in the State of New York in the United States of America and each party hereby consents and submits to the personal jurisdiction of such court, waives any objection to venue in such court and consents to service of process by registered or certified mail, return receipt requested, at the last known address of such party.

WILEY OPEN ACCESS TERMS AND CONDITIONS
Wiley Publishes Open Access Articles in fully Open Access Journals and in Subscription journals offering Online Open. Although most of the fully Open Access journals publish open access articles under the terms of the Creative Commons Attribution (CC BY) License only, the subscription journals and a few of the Open Access Journals offer a choice of Creative Commons Licenses. The license type is clearly identified on the article.
The Creative Commons Attribution License
The Creative Commons Attribution License (CC-BY) allows users to copy, distribute and transmit an article, adapt the article and make commercial use of the article. The CC-BY license permits commercial and non-
Creative Commons Attribution Non-Commercial License
The Creative Commons Attribution Non-Commercial (CC-BY-NC)License permits use, distribution and reproduction in any medium, provided the original work is properly cited and is not used for commercial purposes.(see below)

Creative Commons Attribution-Non-Commercial-NoDerivs License
The Creative Commons Attribution Non-Commercial-NoDerivs License (CC-BY-NC-ND) permits use, distribution and reproduction in any medium, provided the original work is properly cited, is not used for commercial purposes and no modifications or adaptations are made. (see below)
Use by commercial "for-profit" organizations
Use of Wiley Open Access articles for commercial, promotional, or marketing purposes requires further explicit permission from Wiley and will be subject to a fee.
Further details can be found on Wiley Online Library

http://olabout.wiley.com/WileyCDA/Section/id-410895.html

Other Terms and Conditions:

v1.10 Last updated September 2015

Questions? customercare@copyright.com or +1-855-239-3415 (toll free in the US) or +1-978-646-2777.